Universidade de São Paulo
Instituto de Física

Estudo do comportamento da entropia em bilhares

Gabriel Díaz Iturry

Orientador(a): Prof. Dr. Edson Denis Leonel

Coorientador(a): Prof. Dr. Iberê Luiz Caldas

Tese de doutorado apresentada ao Instituto de Física da Universidade de São Paulo, como requisito parcial para a obtenção do título de Doutor em Ciências.

Banca Examinadora:
Prof. Dr. Edson Denis Leonel - Orientador (UNESP/IFUSP)
Prof. Dr. Mario José de Oliveira (IFUSP)
Prof. Dr. Antônio Marcos Batista (UEPG)
Prof. Dr. Luiz Antonio Barreiro (UNESP)
Prof. Dr. Ricardo Luiz Viana (UFPR)

São Paulo
2020

FICHA CATALOGRÁFICA
Preparada pelo Serviço de Biblioteca e Informação
do Instituto de Física da Universidade de São Paulo

Díaz Iturry, Gabriel

Estudo do comportamento da entropia em bilhares. São Paulo, 2021.

Tese (Doutorado) – Universidade de São Paulo. Instituto de Física. Depto. de Física Aplicada

Orientador: Prof. Edson Denis Leonel

Área de Concentração: Física

Unitermos: 1. Caos (Sistemas dinâmicos); 2. Bilhares; 3. Entropia.

USP/IF/SBI-007/2021

University of São Paulo
Physics Institute

Study of entropy behaviour in billiard systems

Gabriel Díaz Iturry

Supervisor: Prof. Dr. Edson Denis Leonel _____
Co-supervisor: Prof. Dr. Iberê Luiz Caldas _____

Thesis submitted to the Physics Institute of the University of São Paulo in partial fulfillment of the requirements for the degree of Doctor of Science.

Examining Committee:
Prof. Dr. Edson Denis Leonel - Orientador (UNESP/IFUSP)
Prof. Dr. Mario José de Oliveira (IFUSP)
Prof. Dr. Antônio Marcos Batista (UEPG)
Prof. Dr. Luiz Antonio Barreiro (UNESP)
Prof. Dr. Ricardo Luiz Viana (UFPR)

São Paulo
2020

A quienes quiero.

Ustedes saben quienes son.

Agradecimentos

Agradezco a mi familia por su paciencia y por el *tiempo propio* que vivimos; a mi orientador Prof. Edson Denis Leonel y coorientador Prof. Iberê Luiz Caldas por brindarme la oportunidad de desarrolar este trabajo, a Matheus Palmero por sus agudas observaciones. A las amistades, antiguas y nuevas, que están ahí por el mundo. Agradezco tambien a la agencia CNPq y al Instituto de Física de USP-São Paulo.

A los que ayudaron en esto.

Resumo

Neste trabalho estudamos como usar o comportamento da entropia para medir o expoente de difusão de um conjunto de condições iniciais em sistemas do tipo bilhar. Os modelos considerados são o Modelo Fermi Ulam Simplificado, o Mapa Padrão e o Bilhar Ovóide. Nos preocupamos com a difusão perto da ilha principal no espaço de fases, onde existe o fenômeno de aprisionamento temporário. Calculamos o expoente de difusão para diversos valores do parâmetro de controle do Mapa Padrão e o Bilhar Ovóide, onde para cada valor a ilha principal tinha uma forma diferente, e mostramos que as mudanças de comportamento no expoente estão relacionadas com mudanças na área da ilha principal. Particularmente, mostramos que toda vez que a área da ilha principal se reduzia abruptamente, devido a destruição de toros invariantes e a criação de pontos fixos hiperbólicos e elípticos, o expoente de difusão cresce. Para investigar melhor a conexão entre o expoente de difusão e a criação de pontos fixos hiperbólicos e elípticos, desenvolvemos um esquema de controle apropriado no Mapa Padrão, com o qual mostramos que fechando os caminhos de fuga das proximidades da ilha o expoente de difusão tornou-se menor. Em seguida, relacionamos os caminhos de fuga com a variedade instável dos pontos hiperbólicos.

Palavras Chaves: Caos, Bilhares, Difusão.

Abstract

In this work we studied how to use the behaviour of the entropy to measure the diffusion exponent of a set of initial conditions in Billiard like systems. The considered models are the Simplified Fermi Ulam Model, Standard Map and the Oval Billiard. We care about the diffusion near the main island in the phase space, where exists the stickiness phenomenon. We calculated the diffusion exponent for many values of the nonlinear parameter of the Standard Map and the Oval Billiard, where for each value the main island has a different shape, then we show that the changes of behaviour in the diffusion exponent are related to changes in the area of the main island. Particularly, we show when the main island's area is abruptly reduced, due to the destruction of invariant tori and consequently creation of hyperbolic and elliptic fixed points, the diffusion exponent grows. To further investigate the connection between the diffusion exponent and the creation of hyperbolic and elliptic fixed points, we developed an appropriate control scheme in the Standard Map, with which we showed that closing paths of escape from the island shore the diffusion exponent became smaller. Then we related the paths of escape with the unstable manifold of the hyperbolic points.

Key Words: Chaos, Billiards, Diffusion.

CONTENTS

Chapter 1

Introduction

1.1 A brief history of nonlinear dynamics, the beginning

In the second half of 17th century Newton was able to mathematically describe the planetary motion of two bodies [1], which until then was known by the empirical Kepler's laws.

New generation of mathematicians and physicists tried to solve the gravitational problem of three bodies without success. At the end of 19th century Poincaré brought a new insight to the problem [2]. Instead of wondering about quantitative aspects, he asked about qualitative description of the problem, as the stability of the motion. With this in mind he developed geometric approximations to analyze the problem. Even though the three body problem was not solvable by looking for *first integrals of motion*, at the end of 20th century Sundman found an analytic series approximation of the solution to the gravitational problem of three bodies for almost all admissible initial conditions [3], later, in 1990, Wang resolved the problem of n bodies [4], again in an analytic series approximation. Both solutions showed up to be of less interest than Poincaré's geometric approach for qualitative aspects, since physically they do not brought new insights to the problem in hands, even more, both series converge very slowly, so not even presented numerical improvement [5].

In the second half of the 20th century the studies in dynamics focused in nonlinear oscillators and applications of those in physics and engineering, applications such as radio, laser, radar among many others. In the theoretical counterpart new methods of

analysis, based on Poincaré's geometric approach, were developed. The use of the computers to perform the calculations allowed to study and experiment with new equations in ways that were impossible before. This kind of experiments yields Lorenz, while studying atmospheric models, to the discovery of chaotic movement in strange attractors [6]. Lorenz found that solutions to the equations he was studying could oscillate in a strange and unpredictable way, even more, starting from close initial conditions the behaviour of the trajectories could be very different.

After Lorenz's discovery many more similar results were found in sciences while studying nonlinear systems. In the 70's Feigenbaum realized there are universal laws governing transition between regular and chaotic behaviour [7]. He proved that two completely different systems can become chaotic in the same way. Besides chaos, nonlinear dynamics also growth due the works done in fractals and synchronization [8].

An important area of research in nonlinear dynamics is in systems described by a Hamiltonian [9]. The system's dynamical variables are canonical conjugate pair of variables, position and momentum. If in the dynamics exist conserved quantities, integrals of movement, it is possible to reduce the number of variables that describe the system. If a Hamiltonian system has as many integrals of movement as position-momentum pairs, it is called of integrable. In many cases, an integrable Hamiltonian system under an arbitrary perturbation leads to chaotic dynamics.

1.2 Objectives and some preliminary concepts

The diffusion problem in phase space for low dimensional classical Hamiltonian systems is very important nowadays from a theoretical point of view [10, 11]. The presence of regular and chaotic trajectories produces different kinds of diffusion for densities of trajectories. Depending on the region in the phase space the diffusion may be normal or anomalous. From a physical point of view, diffusion in phase space is present in many problems, such as the unlimited growth of energy, [1][12, 13, 14], or the study of transport properties from one region of phase space to another region [15, 16], and plasma dynamics [17, 18], among others.

Usually the diffusion is studied as the growth over time of the standard deviation

[1]This phenomenon is some times called Fermi Acceleration, the diffusion is along the energy axis.

of a generalized momentum variable [10, 19, 20, 21], in those studies it is considered that the diffusion along the generalized position, angle like variable, is fast. The growth over time (t) of the standard deviation ($\sigma = Ct^{\Delta}$) is characterized by two variables, a diffusion coefficient (C) and a diffusion exponent (Δ), the most important being the exponent since it allows us to distinguish between anomalous diffusion, when the exponent is different from $1/2$, and normal diffusion, when the exponent is $1/2$. Even though this method gives good results in some cases, like in an almost completely chaotic sea [22, 23], it fails in some other cases, since it is difficult to find the appropriate generalized momentum that it is better suited to describe a specific behaviour in phase space [24, 25]. A particular physical scenario where the momentum method fails, is when exists coexistence of dynamics, regions of regular trajectories arranged in complex structures called Kolmogorov-Arnold-Moser (KAM) islands [26, 27, 28], surrounded by a sea of chaotic trajectories. This complex scenario is described by the KAM Theorem, which states that quasiperiodic motion persists under small perturbations on integrable Hamiltonian systems. Due to the action of the perturbation some invariant curves, tori, are deformed and some are broken becoming pairs of unstable/stable fixed points. Stable fixed points are surrounded by invariant curves forming stability islands, and the set of broken tori form a complex pattern, the Cantori [26, 27, 28, 29].

A method that overcomes the standard-deviation problem was proposed by Scafetta and Grigolini to characterize superdiffusive dynamics. This method, called Diffusion Entropy Analysis (DEA), is known to serve in common diffusion models [30], it is based on the use of entropy behaviour rather than the standard deviation's behaviour. For our purposes, study diffusion in Hamiltonian systems, we adapt this method. Considering the fact that the entropy is invariant under a certain type of variable transformations, as changing from one set of canonical variables to another, we expect that the method works fine in the physical scenarios where finding momentum variables is not feasible.

In this work we will focus in two points:

1. Use measurement of *Entropy* to study *Diffusion* process in *Billiard Systems*.

2. Give empirical explanation of the diffusion regimes encountered.

We will use the Shannon Entropy [31]. This entropy *quantifies the unevenness of a probability distribution* [32]. Some valid remarks about Shannon entropy in the problem at hands are:

- It is in natural units.
- It is not the Thermodynamical entropy, the system is deterministic and not in equilibrium.

The idea of diffusion that we use in this work is *the movement of particles from region of higher concentration to region of lower concentration*. Particularly we will consider trajectories of an ensemble of non-interacting particles, our dynamical models will be deterministic then the ensemble behaviour is completely determined from the initial conditions of its components.

A billiard system is a class of Hamiltonian system. *It consists in free particle moving a N-dimensional closed region suffering collisions with a border*. This system shows the complexity of general low dimensional Hamiltonian systems with simple dynamical laws.

We will specifically focus in using the entropy behaviour to characterize the diffusion around KAM islands; we particularly focus in the subdiffusive behaviour produced by the Cantori.

1.3 Organization of the text

The text is organized as follows:

In chapter 2 we present the dynamical models that will be our working place where we will study the diffusion process. The models are the Standard Map [33, 34] and the Oval Billiard [35]. We give a detailed discussion about the mappings variables and control parameters. We also describe the different kinds of dynamics that they present, i. e. regular, quasiregular and chaotic. We particularly care about showing the KAM islands and in describing the mappings in canonical variables, this last point is important in order to measure the entropy.

Chapter 3 shows how to use the Diffusion Entropy Analysis approach in a Hamiltonian map that we know it presents normal diffusion process, with this we can *establish a methodology to characterize the diffusion exponent* in other scenarios, i. e. around KAM islands. The main result from this chapter is a *relation between* the *diffusion range* of our variables, the *fluctuation size* that ensemble suffers under the dynamics, and the *number of grid divisions* needed to measure the entropy by an histogram.

Having the results from chapter 3 we proceed to *study the diffusion around the KAM islands*, this is done in chapter 4. We proceed to calculate the diffusion exponent for many values of the control parameter both for the Standard Map as for the Oval Billiard, and show there is a correlation between the main island's area and the diffusion exponent. Particularly *we find that when the main island's area is abruptly reduced*, due the destruction of invariant tori and creation of hyperbolic and elliptic fixed points, *the diffusion exponent grows*. Then, *we relate this behaviour with the influence of invariant manifolds associated to the hyperbolic fixed points.*

In chapter 5 we drawn conclusions and discuss our results.

Finally, in chapter 6 we present our perspectives for future research.

Chapter 2

Dynamical models

In this chapter we present a brief description of the dynamical models that we use along the text: The Standard Map and the Oval Billiard. A more complete description and demonstration of the maps is shown in Appendix A and Appendix B.

2.1 Standard Map, the typical first example

Dynamical systems provide mathematical models that help to comprehend different phenomena [36, 37, 9, 38]. In Physics several dynamical systems can be described by a Hamiltonian. Among a variety of possible physical phenomena, the ones described by low dimensional Hamiltonians have a special property, they may present chaotic behaviour even though the deterministic dynamics is simple.

To describe and understand dynamical systems is common to use a *Poincaré's section*. This description gives information about the dynamics in a resumed way, it exploits the existence of symmetries or some geometrical characteristics of the dynamical system, see figure 2.1.

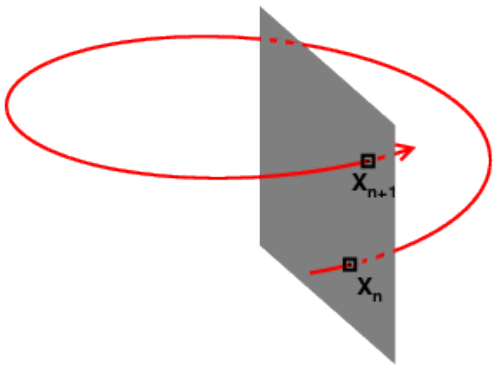

Figure 2.1: Diagrammatic explanation of a Poincaré section in a fictitious system.

In figure 2.1 we show a diagrammatic explanation of a Poincaré section. The trajectory in phase space[1] is described by the red line. Assuming that the trajectory will always cross the gray plane we only care about the points where the red line crosses the plane in a given direction, this gives the map $x_{n+1} = F(x_n)$. A condensed description of the dynamics, the Poincaré section, is achieved by the mapping sequence x_n, x_{n+1}, ...

In Classical Mechanics, the dynamics of a system can be described by a Hamiltonian. The system's phase space is given by canonical conjugate pair of variables, generalized position and momentum. Trajectories in phase space do not cross each other, even more, if in the dynamics exist conserved quantities, integrals of movement, it is

[1]Phase space is a space in which all possible states of a system are represented, it has one dimension for each variable that describes the system.

possible to reduce the dimensions in the representation. If a Hamiltonian system has as many integrals of movement as position-momentum pairs, it is called of integrable. In many cases, an integrable Hamiltonian system under an arbitrary perturbation leads to chaotic dynamics. In this kind of systems is usual to use a Poincaré section, since we can reduce one dimension in the representation of the trajectory, given us a much simpler image of the problem at hands. Since this representation is discretized, i. e. we have a sequence x_n, x_{n+1}, ..., we call it a Poincaré map representation.

A typical example of a Poincaré map of a low dimensional Hamiltonian is given by Chirikov's Standard Map [33, 34]. The unperturbed Hamiltonian describes the free motion of a particle constrained to move in a ring:

$$H_0\left(q,p\right)=\frac{p^2}{2}, \tag{2.1}$$

this is an integrable Hamiltonian system, we have only one pair $[q,p]$ and one conserved quantity, the energy. To this system we add a periodic time dependent perturbation, giving the following Hamiltonian:

$$H\left(q,p,t\right)=\frac{p^2}{2}+k\cos\left(q\right)\sum_{n=-\infty}^{\infty}\delta\left(t-n\right), \tag{2.2}$$

the second term in the right hand side represents the particle being kicked periodically by an external q dependent field, the magnitude of this field is given by the parameter k. If it's value is different from zero, the energy is not longer a constant of movement, thus, this is a nonintegrable Hamiltonian system, characterized by the nonlinearity parameter k. A Poincaré map can be constructed considering the position-momentum pair after each kick, this is the Chirikov's Standard Map, derived in Appendix A:

$$\begin{aligned} p_{n+1} &= p_n+k\sin\left(q_n\right), \\ q_{n+1} &= q_n+p_{n+1}, \end{aligned} \tag{2.3}$$

where q_n and p_n are positions in phase space at iteration n, k is the parameter that controls the nonlinearity, the equation (2.3) gives at each iteration a new position in phase space. In Appendix A is shown that this is an area preserving map. A common[2]

[2]Unless stated otherwise, this will be the case in this Thesis.

procedure is to actually care of q_n and p_n modulo 2π.

A important set of trajectories possibles in the mapping (2.3) are the fixed points, periodic orbits[3] [8]. Since the map is area preserving there are two possible types of fixed points: i) The elliptic ones, who have neutral stability in all directions around them, and ii) the hyperbolic fixed points, who have directions of stability and unstability [8, 39]. From these directions of stability/unstability, are born the invariant manifolds[4], both the stable[5] as the unstable[6]. These invariant manifolds have important properties, i) At each iteration a point in a manifold is mapped to another point in the manifold, ii) they influence the dynamics around them, trajectories tend to align along the unstable manifold, iii) their action is all over the phase space.

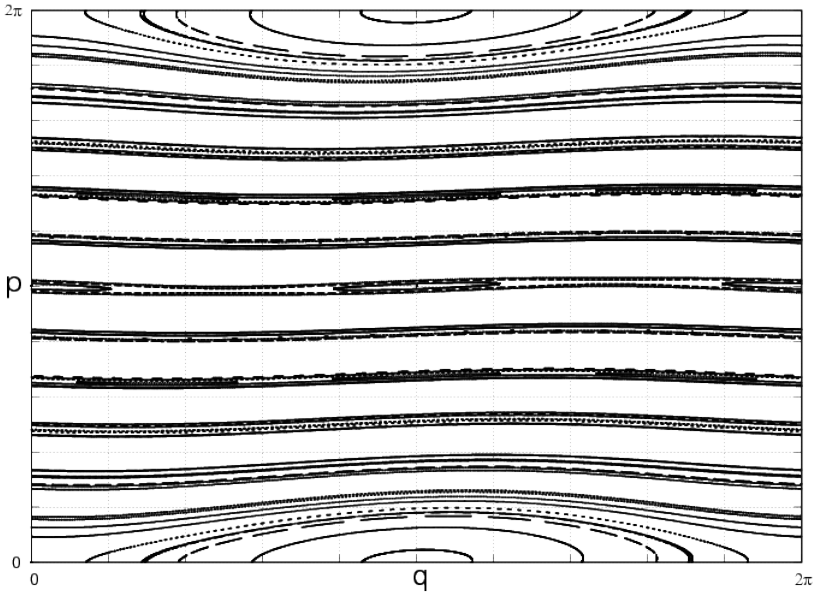

Figure 2.2: Phase space portrait of Standard Map for $k = 0.1$.

[3]The fixed points of period m are the set of solutions that have property $x_0 = F^m(x_0)$.

[4]A manifold is a topological space that locally resembles Euclidian space near each point.

[5]Stable manifold is the invariant set of points that goes to the fixed point when the number of iterations goes to infinity. For a mapping $f\colon X \to X$ the stable manifold of a fixed point $x_0 = f(x_0)$ is the invariant set defined by $W^s(f, x_0) = \{x \in X : f^n(x) \to x_0 \text{ as } n \to \infty\}$.

[6]Unstable manifold is the invariant set of points that goes to the fixed point when the number of iterations of the inverse mapping goes to infinity. For a mapping $f\colon X \to X$ the unstable manifold of a fixed point $x_0 = f(x_0)$ is the invariant set defined by $W^u(f, x_0) = \{x \in X : f^{-n}(x) \to x_0 \text{ as } n \to \infty\}$, where f^{-1} is the inverse of f.

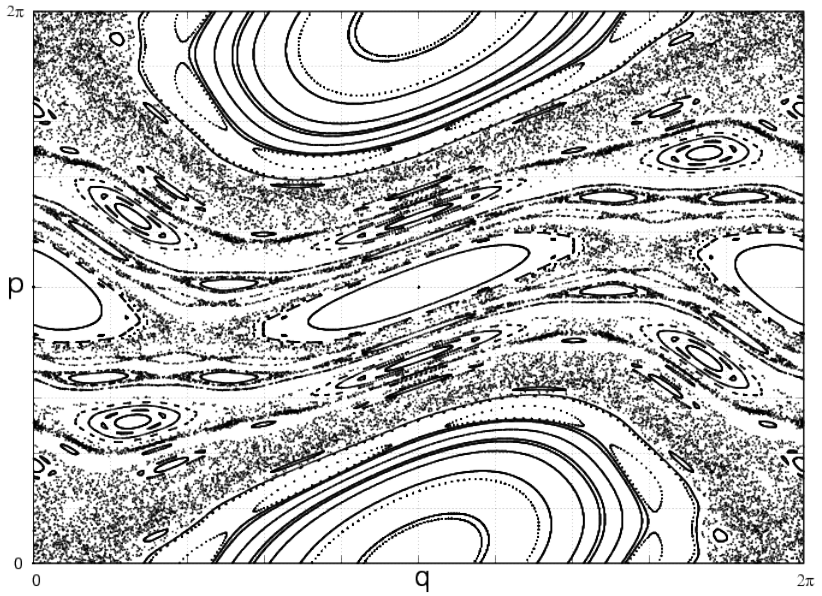

Figure 2.3: Phase space portrait of Standard Map for $k = 1.0$

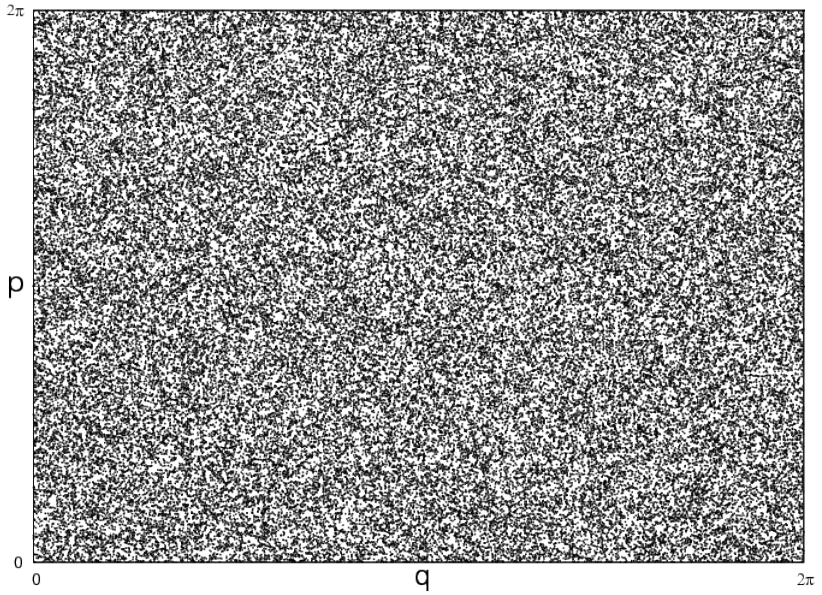

Figure 2.4: Phase space portrait of Standard Map for $k = 9.1$

A portrait of the phase space of the Standard Map 2.3 is given in figures 2.2, 2.3, 2.4 for different values of the parameter k, from very regular (fig. 2.2) to practically

completely chaotic (fig. 2.4), passing by coexistent dynamics[7] (fig. 2.3). For a given set of initial conditions in phase space we applied many times the mapping (2.3) to go from on position in phase space to another position, those positions are drawn as points in the phase space portrait. For values of k where there is coexistence of dynamics, the regions of regular motion are generally formed by *invariant curves*[8] arranged in complex structures called Kolmogorov-Arnold-Moser (KAM) islands[9].

2.2 Billiard systems, hardly pool games

Among many Hamiltonian systems ones of special interest are the billiard systems [40, 41]. They evolve by simple dynamical rules but show all the complexity of general low dimensional Hamiltonian dynamics, they can be integrable, as the circular billiard, ergodic, as the Sinai billiard, or of mixed phase space, as the Oval billiard, see ref [41]. Even more, billiard systems can be used to model some phenomena with direct physical interpretation, as thermometric efficiency, nuclear collisions, transport and others [42]. The most simple one consists of a free particle moving in a N-dimensional closed region suffering collisions with a border. We can also add some special dynamics both in the original *free moving particle region* as in the *collision zone*, for example, the movement of the particle can be influenced by external field forces, and the border, also known as wall, can be moving in a known way, besides that, the collisions can be elastic or inelastic.

The notion of billiard is known since Birkhoff proposed the problem of a spherical particle moving in many directions colliding with a border [43]. Later on, due the work of Sinai in mathematical properties of billiards of dispersing wall [44], and also Krylov's exhaustive work in the same systems [45], a new period of billiard analysis begun.

The oval billiard, introduced M. Berry in [35], is nowadays a common billiard sys-

[7] Mixed dynamics in the sense that chaotic, periodic and quasi periodic dynamics coexist.

[8] Invariant under the action of the map, i. e. a set of points that is over an invariant curve will always be over it when we iterate our mapping. The motion of these points is quasiperiodic so they draw a curve in the phase space portrait. They are also known as invariant tori.

[9] KAM Theorem states that quasiperiodic motion persist under small perturbations on integrable Hamiltonian systems. Due the action of the perturbation some invariant curves, tori, are deformed and some are broken becoming pairs of unstable/stable fixed points. Stable fixed points are surrounded by invariant curves forming stability islands, and the set of broken tori form a complex pattern, the Cantori [26, 27, 28, 29].

tem well studied. The radius of the boundary, in polar coordinates, is given by

$$R\left(\theta,\epsilon,p\right) \;=\; 1+\varepsilon\cos\left(p\theta\right). \tag{2.4}$$

The parameter $\varepsilon \in [0,1)$ controls the deformation of the circle, the non linearity, p is an integer number and $\theta \in [0,2\pi)$ is the polar angle. A trajectory is shown in figure 2.5.

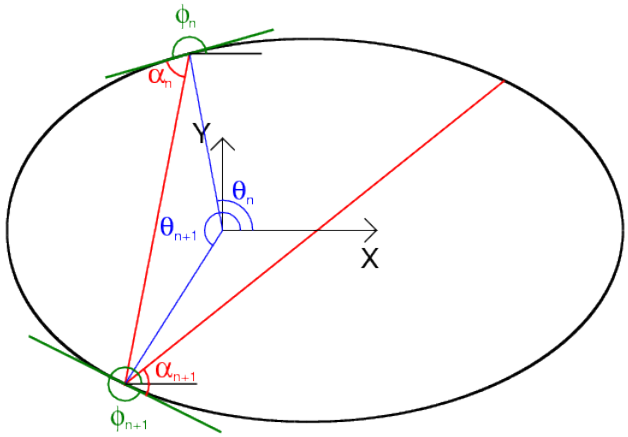

Figure 2.5: Trajectory of a particle inside an oval billiard with $p = 1$ and $\varepsilon = 0.3$

In figure 2.5 we show an example of a particle's trajectory inside the oval billiard, we consider elastic collisions, then, the velocity component tangent to the boundary is conserved while the normal component changes sign. Between collisions the particle moves in straight lines, *free moving particle*. A Poincaré section of this trajectory can be constructed if we collect data at each collision of the particle with the wall. In this case we care about two variables, the angle θ of collision, and the angle α that makes the trajectory with the tangent to the boundary. This set of variables give a resumed description of the trajectory.

In Appendix B we describe an algorithm used to perform the simulation of the particle's movement. Starting from the coordinates (θ_n, α_n) we find the particles position, $x_n = R\left(\theta_n,\epsilon,p\right)\cos(\theta_n)$, $y_n = R\left(\theta_n,\epsilon,p\right)\sin(\theta_n)$, and velocity, $v_{x,n} = \cos(\alpha_n + \phi_n)$

$v_{y,n} = \sin(\alpha_n + \phi_n)$. With this information we calculate the time t_n to the next collision between the particle and the border, for this we consider a free particle movement, once we have the time t_n, we calculate the position of the collision, x_{n+1}, y_{n+1}, and the new velocity after the collision, $v_{x,n+1}$, $v_{y,n+1}$, considering elastic collisions. With this we find the new coordinates (θ_n, α_n).

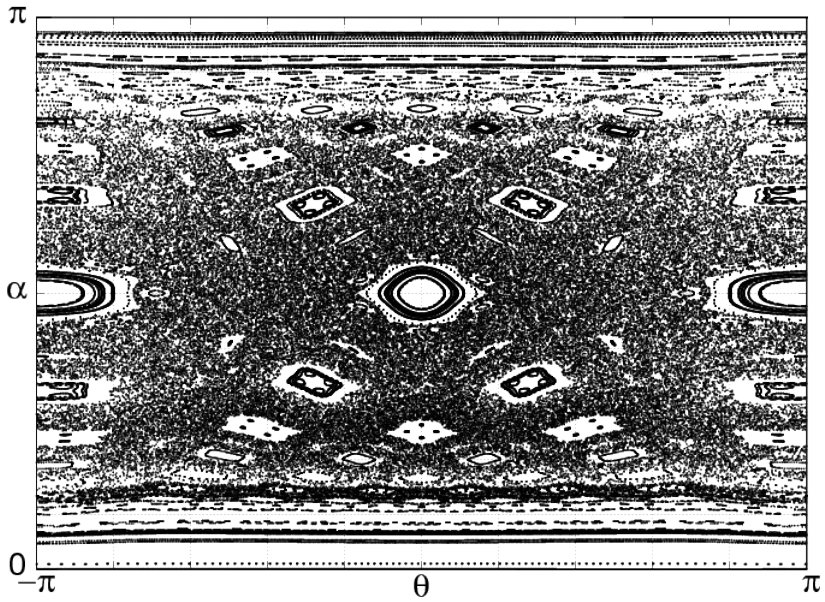

Figure 2.6: Portrait of the Poincaré section of oval billiard with parameters $p = 1$ and $\varepsilon = 0.3$.

Figure 2.6 shows the Poincaré section portrait of the oval billiard for the parameters $p = 1$ and $\varepsilon = 0.3$. Our Poincaré section is described by the variables θ and α shown in figure 2.5. For a given set of initial conditions we follow the trajectories and write the variables α, θ after each collision with the billiard's wall. We see it has similar structures as those shown in figure 2.3 of the Standard Map, i. e., a chaotic sea surrounding KAM islands. In this case the *main island* belongs to a periodic orbit, we care about the island centered in $\alpha = \frac{\pi}{2}$ and $\theta = 0$.

The pair (θ_n, α_n) is not set of canonical conjugate variables, then, its mapping is not area preserving. We have to transform to Poincaré-Birkhoff coordinates [43] to have an area preserving map, these are given by the arc-length, s_n, and the tangential velocity, v_n, to the impact point at the n^{th} collision.

The tangential velocity, v_n in the n^{th} collision is given by:

$$v_{n+1} = \cos(\alpha_{n+1}). \tag{2.5}$$

The arc-lenght s_n at the n^{th} iteration can be found by the integral:

$$s_n = \int_0^{\theta_n} \sqrt{R(\theta)^2 + \left(\frac{dR(\theta)}{d\theta}\right)^2} d\theta, \tag{2.6}$$

where the radius $R(\theta)$ is parameterized by the angle θ, Eq. (2.4). Considering $p = 1$ and doing some algebra we arrive to

$$s_n = \frac{2}{1+\varepsilon} \int_0^{\frac{\theta_n}{2}} \sqrt{1 - \frac{4\varepsilon}{(1+\varepsilon)^2} \sin^2(u)} du, \tag{2.7}$$

which can be written in terms of the incomplete elliptic integral of second type, $E(\phi, k)$, [48], the numerical value can be computed efficiently using the subroutines provided by [49]. The new mapping (s_n, v_n) to (s_{n+1}, v_{n+1}) it is given by:

$$\begin{aligned} s_{n+1} &= \frac{2}{1+\varepsilon} E\left(\frac{\theta_{n+1}}{2}, \frac{2\sqrt{\varepsilon}}{1+\varepsilon}\right), \\ v_{n+1} &= \cos(\alpha_{n+1}). \end{aligned} \tag{2.8}$$

In Appendix A we show that this is an area preserving mapping.

These models, Standard Map and Oval Billiard, will be used in the subsequent Chapters as examples of mappings that present anomalous diffusion. We will study their diffusion processes, characterize the diffusion exponent, and describe the physical scenario that leads to such class of anomalous diffusion.

Chapter 3

Diffusion, an entropy approach

In this chapter we present the Diffusion Entropy Analysis approach, developed in [30]. We show how to make this approach suitable to our mappings, then we apply this adaptation to a known normal diffusion process. With this we establish an important relation, eq. (3.8), and a methodology to measure the diffusion exponent, which will be used in other diffusive scenarios in chapter 4.

3.1 Diffusion

The diffusion problem in phase space for low dimensional classical Hamiltonian systems is very important nowadays from a theoretical point of view [10, 11]. The presence of regular and chaotic trajectories produces different kinds of diffusion for densities of trajectories. Depending on the region in the phase space the diffusion may be normal or anomalous. The diffusion in phase space can be used in many problems, such as the unlimited growth of energy, [1][12, 13, 14], or the study of transport properties from one region of phase space to another region [15, 16].

Usually the diffusion is studied as the growth over time of the standard deviation of a generalized momentum variable [10, 19, 20, 21]. In those studies it is considered that the diffusion along the generalized position, angle like variable, is fast. The growth over time, t, of the standard deviation, σ, is characterized by two variables, a diffusion

[1]This phenomenon is some times called Fermi Acceleration, the diffusion is along the energy axis.

coefficient D and a diffusion exponent Δ:

$$\sigma \;=\; Dt^{\Delta}. \tag{3.1}$$

The important variable is the diffusion exponent since it allow us to distinguish between normal diffusion, when the exponent is $1/2$, subdiffusion, when the exponent is less than $1/2$ and superdiffusion, when the exponent is higher than $1/2$.

Even though characterize the diffusion exponent via eq. (3.1) gives good results in some cases, like in an almost completely chaotic sea, see figure 3.1, it fails in some other cases, since it is difficult to find the appropriate generalized momentum that it is better suited to describe a particular behaviour in phase space[2] [24, 25], like around KAM islands, see figure 3.2.

3.1.1 Examples of Diffusion in Maps

Normal diffusion in Hamiltonian systems can be exemplified by the Simplified Fermi-Ulam Model [37, 13], the mapping is:

$$\begin{aligned} \phi_{n+1} &= \left[\phi_n + \frac{2}{V_n}\right] \mod (2\pi)\,, \\ V_{n+1} &= \left\|V_n - 2\epsilon \sin\left(\phi_{n+1}\right)\right\|. \end{aligned} \tag{3.2}$$

This model consists of a classical particle of unit mass, suffering successive elastic collisions in a confined region of one unit of longitude bounded by two walls, one fixed and the other capable of exchange energy with the particle, affecting the particle's velocity V, this depending on which phase ϕ it is the wall. The term $\frac{2}{V_n}$ is the time between collisions and $-2\epsilon \sin\left(\phi_{n+1}\right)$ gives the gain or loss of the particle's velocity/energy in each collision. The absolute value in the velocity is to reinject the particle in the correct direction after each collision, i. e. towards the fixed wall. Although this map is not written in *position-momentum* variables it is area preserving. A detailed explanation of how to obtain the mapping (3.2) and the proof that is area preserving is given in Appendix A.

[2]The canonical transformation might not be obvious and only reachable after an iterative numerical procedure.

For a given value of the control parameter ϵ, we apply the mapping (3.2) to a set of 1×10^6 points, these points correspond to initial conditions that approach an initial probability density, indicated by a small circular red area in the bottom of the map shown in figure 3.1a. After iterating the map, the new positions of the points give us an approach of the new probability density indicated in figure 3.1b, with this we can study the time evolution of the probability density, see figure 3.1.

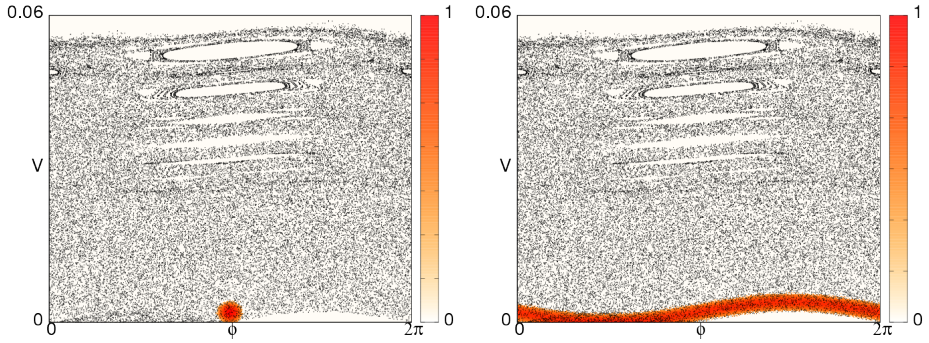

(a) $n = 0$

(b) $n = 1$

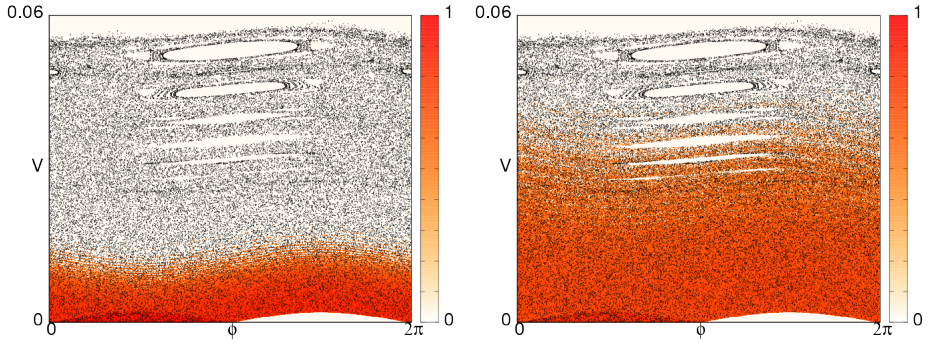

(c) $n = 10$

(d) $n = 100$

Figure 3.1: Plot of the behaviour of the diffusion process, measured by the probability density, in a chaotic region of phase space for the Simplified Fermi-Ulam Model $\epsilon = 0.001$, for different numbers of iterations n. The orange-white color scale represents the density of points in phase space. The subplots (a) to (d) shows the diffusion process.

We see in figure 3.1 that the initial distribution ($n = 0$ in figure 3.1a) is centered around a point, and after only one iteration it spreads out totally along the ϕ axis ($n = 1$ in figure 3.1b). In the next iterations the points diffuse along the V axis while remaining almost spread along ϕ axis ($n = 10$ and $n = 100$ in figure 3.1c and 3.1d).

To show an anomalous diffusion process we will use a variant of the Standard Map

given by:

$$\begin{aligned} p_{n+1} &= p_n + k \sin(q_n), \\ q_{n+1} &= q_n + p_{n+1} + \pi. \end{aligned} \tag{3.3}$$

This map is the same as the typical Standard Map (2.3) just with a translation in the p variable in order to have the main island at the middle of the phase space, near this island there is anomalous diffusion as shown in figure 3.2.

Again we apply the mapping to a set of 1×10^6 points and look at the evolution of the probability density, see figure 3.2.

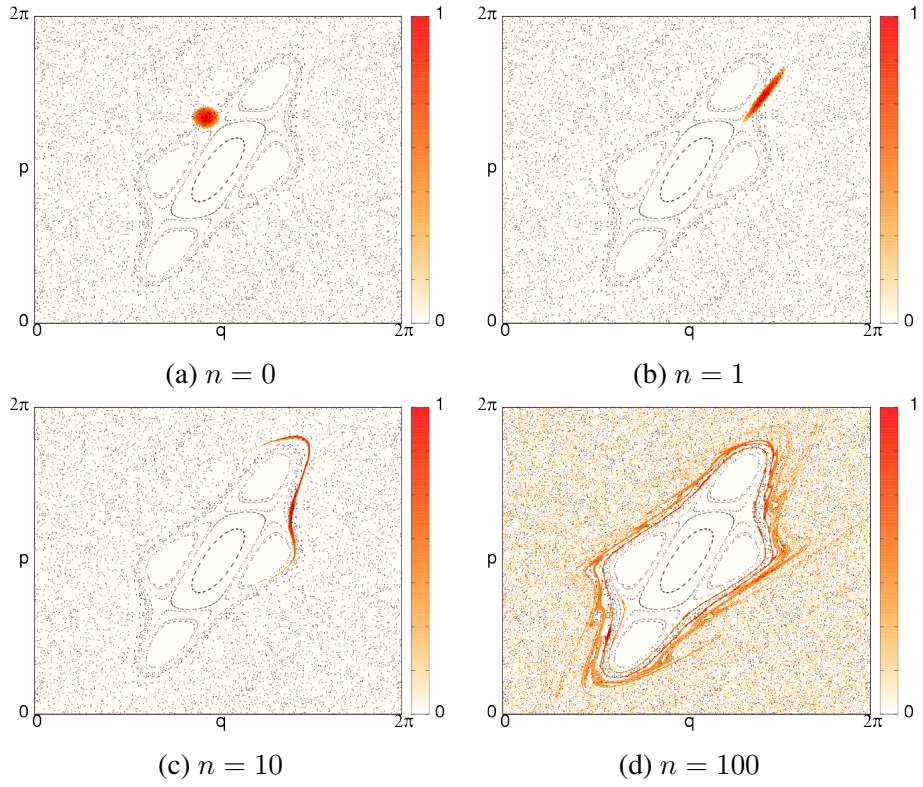

(a) $n = 0$ (b) $n = 1$

(c) $n = 10$ (d) $n = 100$

Figure 3.2: Plot of the behaviour of the diffusion process, measured by the probability density, in a chaotic region of phase space for the Standard Map $k = 2.3$, for different numbers of iterations n. The orange-white color scale represents the density of points in phase space. The subplots (a) to (d) shows the diffusion process.

It is possible to see in figure 3.2 that the probability distribution spreads along the shore of the KAM islands and then diffuses outwards. We can observe that the diffusion

process is not homogeneous, there are preferred channels along which the trajectories leak to the chaotic sea. Even more, this leaking is slow so we are seeing a subdiffusion process.

Find the appropriate canonical variables for this problem is not an easy task, the action/angle variables must be related to the island's invariant curves, i. e. the angle variable tells the position over the invariant curve and the action variable says which invariant curve we are in, see [24, 25]. Since the Shannon entropy is invariant under canonical coordinate transformations, in the next section, we will use it to characterize the diffusion exponent by means of the analysis proposed by Scafetta and Grigolini in [30].

3.1.2 Diffusion Entropy Analysis

The Diffusion Entropy Analysis (DEA), is a method to calculate the diffusion exponent in a variety of diffusive scenarios [30]. To apply this method we need an ensemble of trajectories, from this ensemble we estimate a probability density and it's entropy. Then, analyzing the entropy behaviour we determinate the diffusion exponent. The key to this method is assume an scaling behaviour over time of the probability density of trajectories:

$$\rho\left(x,n\right) \;=\; \frac{1}{n^{\delta}}F\left(\frac{x}{n^{\delta}}\right), \tag{3.4}$$

where δ is a scaling exponent, which later on is defined as the diffusion exponent, x represents a position, n is the iteration number, i. e. the time, and ρ is the probability density near x, this probability varies at each iteration n. The knowledge of the probability density allows us to calculate the entropy easily. The Shannon entropy [31] is given by

$$S \;=\; -\int \rho \ln\left(\rho\right) dx, \tag{3.5}$$

applying eq. (3.4) to last equation we find the relation between entropy and number of iteration[3]:

$$S = A + \delta \ln(n), \tag{3.6}$$

According to the work of Scafetta and Grigolini, ref [30], the diffusion exponent can be defined by equation (3.6), instead of equation (3.1) for the standard deviation. They demonstrated that their definition and method gives better results than standard deviation methods, particularly in some cases of superdiffusion where the standard deviation is not even mathematically defined [4] [30].

To actually use equation (3.5) in our numerical experiments we have to discretize the phase space. In all this work we choose to use a regular $I \times J$ two dimensional grid. After each iteration of a given mapping, we count how many points are inside each box of the grid and construct an histogram, this is our discretized approximation of the probability density. The integral over space in the definition of the Shannon entropy, eq. (3.5), is numerically given by:

$$S = -\sum_{i=1}^{I}\sum_{j=1}^{J} h_{ij} \ln(h_{ij}), \tag{3.7}$$

were the histogram is described by the variables h_{ij} of each box in the grid, with the normalization condition that the sum of all the $[h_{ij}]$ must be one.

In [30] they also give a recipe to select the grid box size, they deal with random walks, where each particle changes position at each time, the fluctuation in the position is given by

$$\xi_i = x_{i,n} - x_{i,n-1},$$

where $x_{i,n}$ is the position of the i^{th} particle at time n. According to [30], the grid box size must be a fraction of the standard deviation of the fluctuations[5] ξ.

[3] In Appendix C we show a detailed demonstration of this passage.

[4] This happens when the probability distribution does not have a first or second moment.

[5] Whose value is independent of time in random walk models [30].

3.1.3 Entropy approach in the Simplified Fermi Ulam Model

Recall equations (3.2), Simplified Fermi Ulam Model, and the diffusion process shown in figure 3.1, we star with an ensemble of points near $V = 0$ and apply the mapping equations in order to get an ensemble of trajectories. To apply the DEA method to this ensemble we need to approximate the probability density function, to do this we divide a section of phase space, shown in figure 3.1, in a regular grid with I (horizontal divisions) $\times J$ (vertical divisions). In this grid, at each iteration, we construct the histogram $[h_{ij}]$ which tells the percentage of points in each grid box, then we measure the Shannon entropy and use equation (3.6).See figure 3.3.

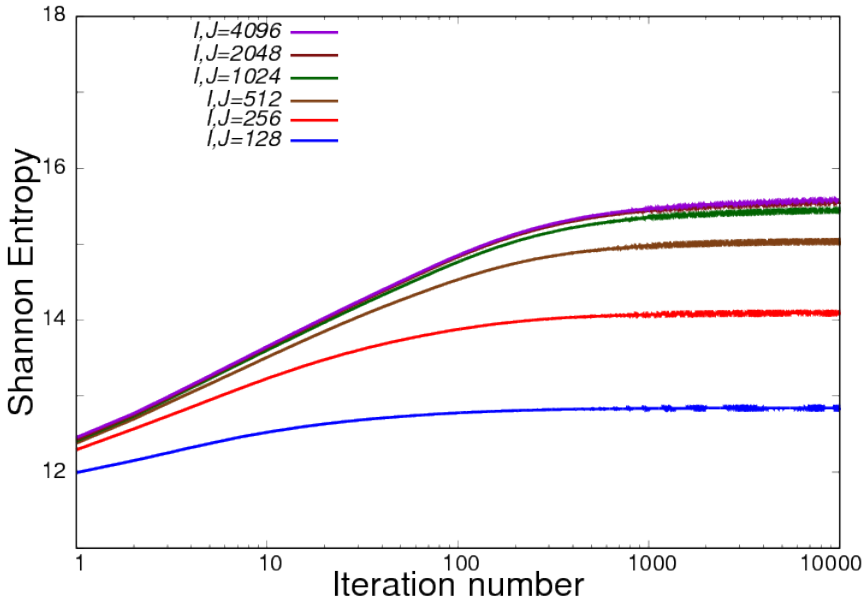

Figure 3.3: Plot of the entropy vs. iteration number. Changing the number of divisions, I, J, in the grid gives different behaviour of entropy over time. We use the Simplified Fermi-Ulam Model with $\epsilon = 0.001$.

In figure 3.3 we see the entropy behaviour for different grid divisions (from $I, J = 4096$ to $I, J = 128$). All curves present two common features, i) the diffusive regime of the dynamics, corresponding to a linear growth shown by each curve, in this regime the particles diffuses in the V direction, ii) that happens until the particles are almost uniformly distributed in the chaotic sea, corresponding to the final plateau reached by each curve.

From [50, 22, 23] we know that for an ensemble of points near to $V = 0$ and small number of iterations, the diffusion process is mainly uniform in the V direction with diffusion exponent δ near to 0.5. Of all curves shown in figure 3.3 the ones that give a δ closer to 0.5 in the diffusive regime, are shown in figure 3.4

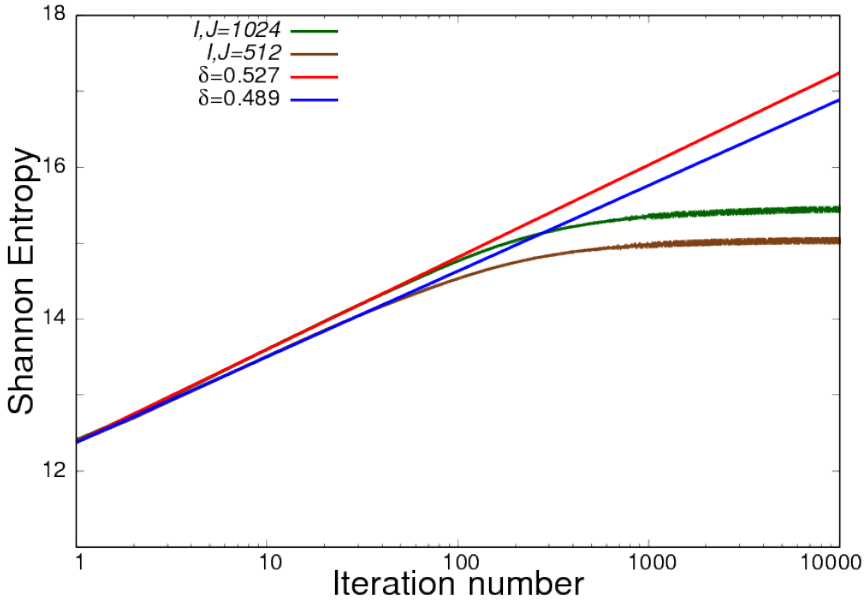

Figure 3.4: Plot of the entropy vs. iteration number. Changing the number of divisions in the grid gives different behaviour of entropy over time. We use the Simplified Fermi-Ulam Model with $\epsilon = 0.001$. We also show the value of the diffusion exponent δ after performing a fit with function $S = A + \delta \ln(n)$ in the diffusive regime.

In figure 3.4 we show the entropy curves that give a fitted δ near to 0.5, as expected from theory [50, 22, 23]. These curves are the ones with $I, J = 1024$ (that gives $\delta = 0.527$) and $I, J = 512$ (that gives $\delta = 0.489$).

From [23], we know that the standard deviation of the fluctuations in the V direction is $\sqrt{2}\epsilon$, from [22] we know that the diffusion range goes from $V_{min} = 0$ to $V_{max} = 2\sqrt{\epsilon}$. The division $\frac{2\sqrt{\epsilon}}{\sqrt{2}\epsilon}$, i. e. *diffusion range* over *fluctuation size*, gives the value 44.72, then, when I, J are one order bigger than this value ($I, J = 512$ in this case), the grid box size is appropriate to calculate the diffusion exponent. We have the empirical relation:

$$10\,\frac{diffusion\ \ range}{fluctuation\ \ size} \quad \sim \quad grid\ \ divisions. \tag{3.8}$$

A detailed description of the scaling (3.4) and its relation with anomalous diffusion it is shown in Appendix C. Demonstration of equation (3.6) and a discussion of its validity in our models is also given in the same appendix. A short review of the physical reasons of the entropy growth and its relation with the time irreversibility is given in Appendix D.

Chapter 4

Results

In this chapter we show some results obtained while studying the entropy behaviour in the standard map. We focus on the diffusion exponent near the main island, and its possible relation with the island's area. Let us remember that the map under study is the following one:

$$\begin{aligned} p_{n+1} &= p_n + k \sin(q_n), \\ q_{n+1} &= q_n + p_{n+1} + \pi. \end{aligned} \tag{4.1}$$

Since we are interested in studying the diffusion behaviour near the islands, anomalous diffusion, we first have to find the main island shore, then pick many initial conditions along it, initial probability distribution, after that we have to iterate the mapping for all the conditions, calculating the entropy at each iteration, and finally, find the diffusion exponent by relation (3.6), as done in figure 3.3.

4.1 Navigating through the chaotic sea

We use the following procedure to get near the main island. We know there is an hyperbolic fixed point at coordinates $q = 0, p = \pi$. Near this point exist chaos, choosing many initial conditions in this region we know they will expand all over the chaotic sea after many iterations of the mapping (4.1). Then we separate the regions visited by the points and the regions that were not visited, see figure 4.1.

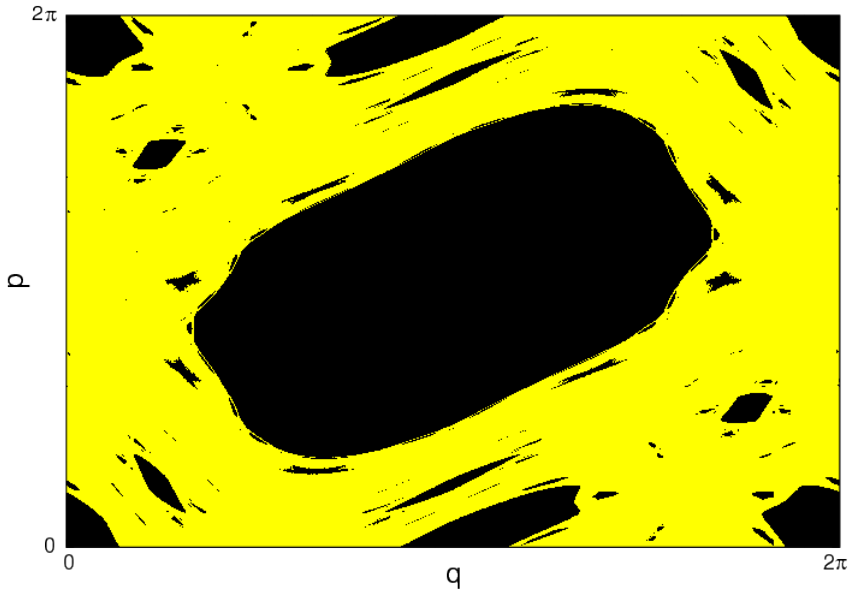

Figure 4.1: Separation the sea of chaos, yellow color, from the regular islands, black color, in the Standard mapping for $k = 1.31$.

To construct figure 4.1 we divided the phase space in a grid of 4096×4096. We choose 1×10^7 initial conditions near the point $[0, \pi]$. For each initial condition we discarded 1×10^3 iterations of the map to give time to the points to get near the islands. Then we iterated 1×10^7 times the mapping, and if any of the points were inside a box of our grid, we assigned a yellow color for that box, if after all iterations no point happened to be inside a box it was assigned a black color. In this way we have an approximation of the chaotic sea and islands in the given grid.

The main island's center is an elliptic fixed point of coordinates $q = \pi$, $p = \pi$. This point is inside a black box in figure 4.1, selecting all the black boxes that are connected, i. e. that are first nearest neighbours, starting from that one, we are able to find an approximation of the main island by a black region of simple connected boxes. An approximation of the mains island's area is given by dividing the number of black boxes that compound this region by 4096×4096 and multiplying by $(2\pi)^2$.

4.2 The shore of the main island

After navigating the chaotic sea we are near the shore of the main island, now we want to get closer, to do this we will investigate the rotation number of a set of orbits.

We consider the elliptic fixed point of coordinates $q = \pi$, $p = \pi$, center of the main island, as our reference point and the ray $q > \pi$, $p = \pi$ as our polar axis and calculate, after each iteration n, the angle θ_n that an orbit has with the polar axis. The rotation number is defined as:

$$r = \lim_{N\to\infty} \frac{\sum_{n=0}^{N} \theta_n}{N}. \tag{4.2}$$

In practice we pick $N = 1000$, but we calculate the rotation number for the same orbit for 1×10^6 iterations, i. e., we have 1000 rotation numbers for the same orbit, if this is a quasiperiodic orbit these rotation numbers must be almost equal, then we expect that for a single quasiperiodic orbit these rotation numbers have a Gaussian distribution with small standard deviation , σ, and small range between the maximal and the minimal rotation numbers found for the same orbit, r_{range}. On the other hand, if the orbit is chaotic we expect that the standard deviation and the range to be big because r does not converge.

To find the shore of the main island first we take the coordinate q_i of the first yellow box that has $q > \pi$ and $p = \pi$ in figure 4.1. Then we choose initial conditions with $p_0 = \pi$ and different values of q_0 around q_i, we take care that the minimal q_0 is actually inside the island, this will be of use later on. For each one of this initial conditions we analyze the rotation number statistics as described in the last paragraph. The results are shown in figure 4.2.

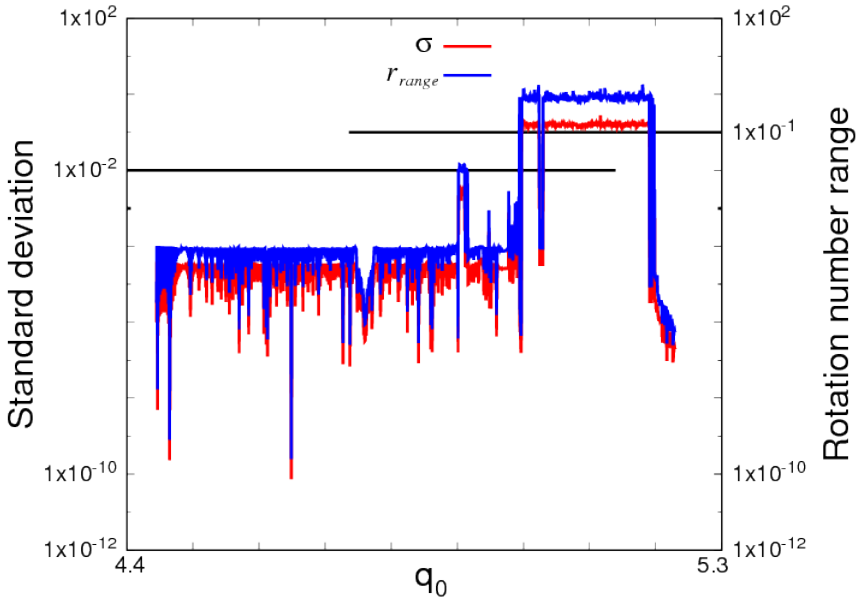

Figure 4.2: The horizontal axis gives the orbit initial q_0 coordinate, p_0 is always π. For each initial condition we calculate the rotation number 1000 times at intervals of 1000 iterations and analyze its distribution. The vertical axis shows the standard deviation σ and rotation number range r_{range} of those distributions, we also show the horizontal cuts $\sigma = 1 \times 10^{-2}$ and $r_{range} = 1 \times 10^{-1}$. The model under study is the Standard Map with $k = 1.31$

In figure 4.2 we show the rotation number statistical behaviour for different initial conditions. The horizontal axis gives the orbit initial q_0 coordinate, p_0 is always π. For each initial condition we iterate the Standard map 1×10^6 times and calculate the rotation number by means of equation (4.2) considering $N = 1000$, obtaining 1000 rotation numbers for each initial condition. Then we analyze the distribution of those 1000 rotation numbers, the vertical axis shows the standard deviation and the range between the maximal and the minimal rotation numbers. To separate quasiperiodic and chaotic behaviours we perform the cuts in $\sigma = 1 \times 10^{-2}$ and $r_{range} = 1 \times 10^{-11}$, meaning that any orbit that has both statistical measures above the cuts is considered chaotic, otherwise is considered quasiperiodic.

From these results we care about the chaotic orbit that has the minimum q_0 for the

[1]The value of these cuts were chosen empirically from observing trajectories in phase space, there is not additional significance in these numbers.

interval considered, we call this value q_{0c}[2]. Once we have this coordinate we save the first 1000 iterations of the map starting from $[q_{0c}, \pi]$, then we add a small perturbation to each one of those 1000 iterations until we have an array of 1×10^6 points, this array of coordinates will be our initial conditions that approach our initial distribution, they will spread in the phase space and we will use them to calculate the diffusion exponent by means of equations (3.6) and (3.7), see figure 4.3.

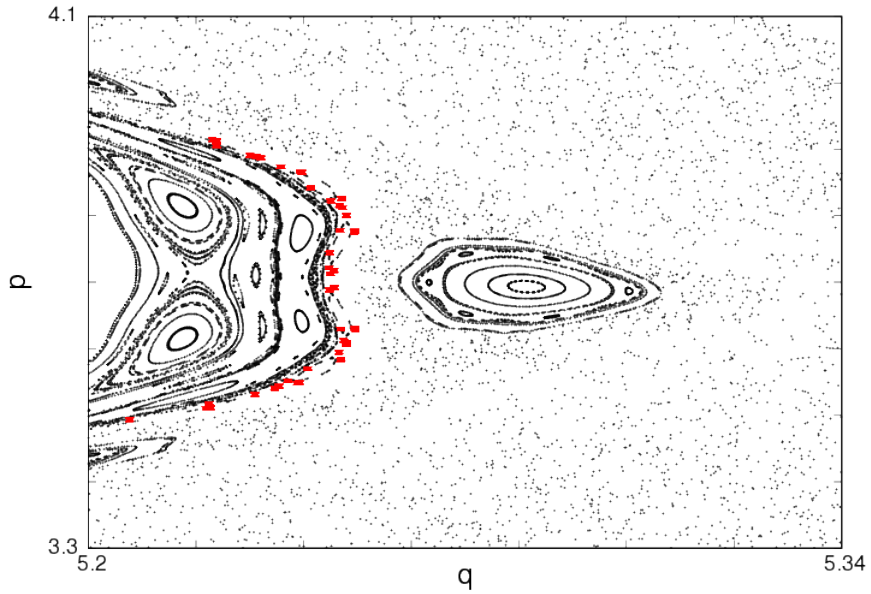

Figure 4.3: Phase space portrait of Standard Map for $k = 1.31$. The red points are the initial coordinates that will spread in phase space and will be used to calculate the diffusion exponent.

Figure 4.3 shows in red the initial condition to be used with equations (3.6) and (3.7) to find the diffusion exponent δ, we observe that they are close to the islands shore and distributed around it, but not uniformly, we need to perform some iterations until they spread along the island, see figure 4.4.

The next step to be taken before been able to measure the diffusion exponent is to define the grid box size, we will use the relation (3.8). We know that the *diffusion range* is 2π for both q as p. To estimate the value of *fluctuation size* we need to know how much does our distribution changes in one iteration, this can be done in the following way; i)

[2]We know that we always will be able to find it since the minimal of all q_0 is quasiperiodic and also q_f marks a yellow box, i. e., chaotic region.

Perform a map iteration on our initial conditions. Even if the i^{th} point jumps far away from its starting position after one iteration, say $x_{i,n} \to x_{i,n+1}$, some other point, say the j^{th}, will land near the starting position of the i^{th} point, $x_{j,n+1} \sim x_{i,n}$; ii) For each one of our initial points $[x_{i,n=0}]$ we search for the $x_{j,n=1}$ points such that $x_{j,n=1} \sim x_{i,n=0}$, then we iii) define the fluctuation at the $n = 1$ iteration as $\xi_{i,n=1} = x_{j,n=1} - x_{i,n=0}$, if we do the same a couple more of iterations, ten iterations in our case, we can iv) approximate the *fluctuation size* as the standard deviation of the $[\xi_{i,n}]$ fluctuations. Observe that this approximation is valid for orbits that are near the main island as our initial distribution is around its shore. In our case we find that $10\ \frac{diffusion\ \ range}{fluctuation\ \ size} = 4856.2$, then we divide our space in $I \times J = 4096 \times 4096$ boxes of equal size. With this grid choice we calculate the Shannon Entropy as shown in figure 4.4.

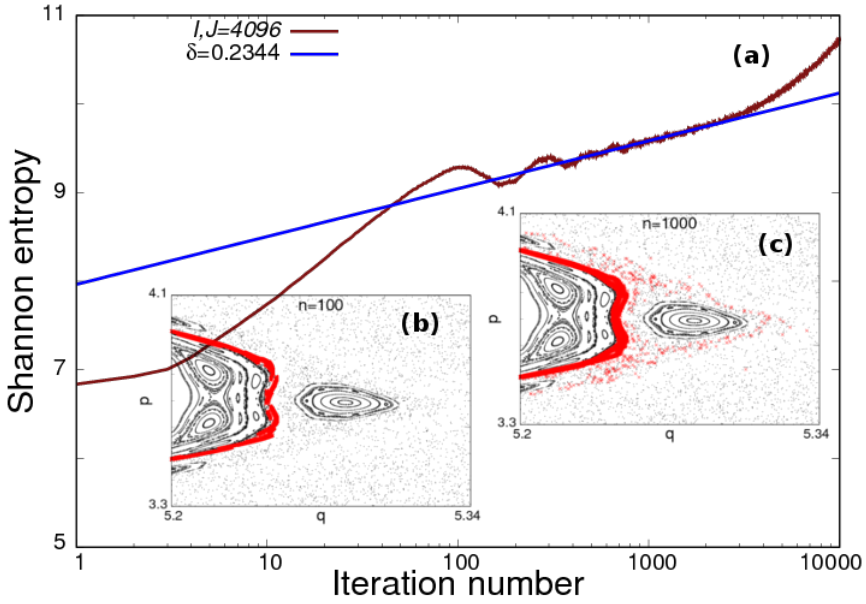

Figure 4.4: Plot of the entropy vs. iteration number for $k = 1.31$. In subfigure (a) we can see that the entropy has three growth regimes, i) in the first 100 iterations the distribution spreads along the main island, subfigure (b), ii) then for 3000 iterations slowly leaks out through the Cantori, subfigure (c), iii) finally more of the distribution is outside the Cantori and rapidly spreads in the chaotic sea.

We show in figure 4.4a the entropy behaviour as the time passes. We can recognize three growth regimes: i) First the distribution quickly spreads along the shore of the main island, this is a fast process equivalent to the spreading in the phase direction in

the SFMU, shown in the transition from figure 3.1a to figure 3.1b. We can appreciate this in the sub-figure 4.4b, that shows how is distributed our ensemble of trajectories after $n = 100$ iterations. ii) The second regime is a slow one, the distribution leaks through the Cantori, see sub-figure 4.4c, this is a regime of subdiffusion, the one where we measure the diffusion exponent, the numerical fit is shown in a blue line, the value of δ is 0.2344. iii) In the third regime more of the distribution is outside the Cantori and rapidly spreads in the chaotic sea. A fourth regime, not shown in figure 4.4, exists, when the ensemble of trajectories is almost uniformly distributed in the chaotic sea, similar to figure 3.4, the entropy reaches a plateau.

4.3 Diffusion exponent and Area

Now that we know how to measure the diffusion exponent δ in the subdiffusive regime for a given parameter k, we want to understand how does δ depends on the value of k. To do this we measure the diffusion exponent for 101 different values of the parameter equally spaced from $k = 1.31$ to $k = 2.31$, see figure 4.5

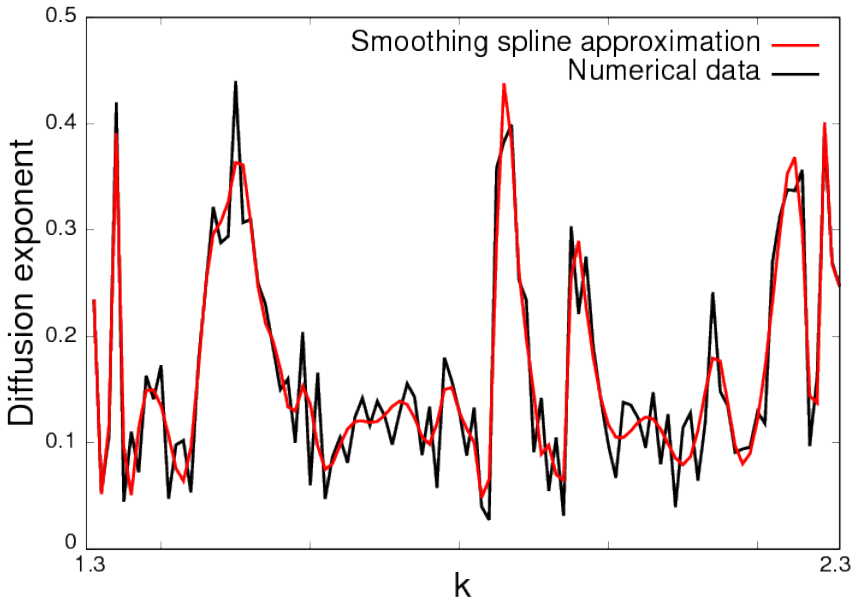

Figure 4.5: Plot of the Diffusion exponent vs. parameter k of Standard Map. The black line represents the numerical data obtained after the power law fitting and the red line is an quintic spline smoothing approximation to the numerical data.

In figure 4.5 we see the behaviour of the diffusion exponent when the parameter k changes. Since this behaviour is very noisy, in part due the election of initial probability distribution, we perform a quintic spline smoothing approximation to the data [51]. With this is possible to appreciate more easily the tendency of the data, i. e. growth and decay of δ. Next we will try to relate the diffusion exponent to some characteristic of the main island, we choose to measure the area[3] of it for all the given values of k, see figure 4.6.

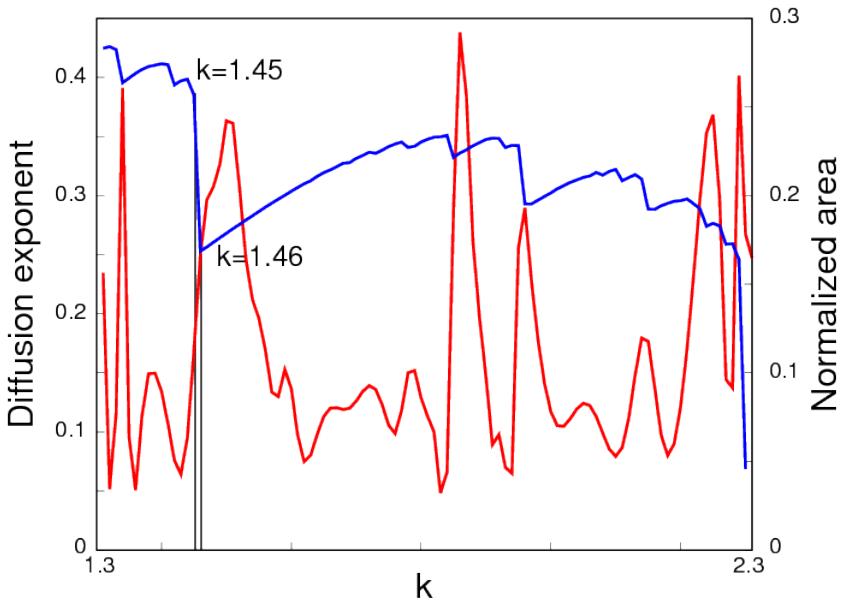

Figure 4.6: Plot of the diffusion exponent, red line, and normalized area of the main island, blue line vs. parameter k of Standard Map. The normalized area is the area of the main island divided by the area of the entire phase space.

It is possible to see in figure 4.6 that every time the area decreases abruptly the diffusion exponent increases. Then the area grows, while the exponent decreases, until a critical value when the area abruptly decreases once more, with its corresponding increase in the diffusion exponent. We mark two values of k figure 4.6, at this interval happens the biggest decrements in the area, for the values of k considered, and we show in figure 4.7 what is happening with the main island at this particular values of k.

[3]The area is measured by the number of black boxes that compound it times $(2\pi)^2$ divided by 4096×4096.

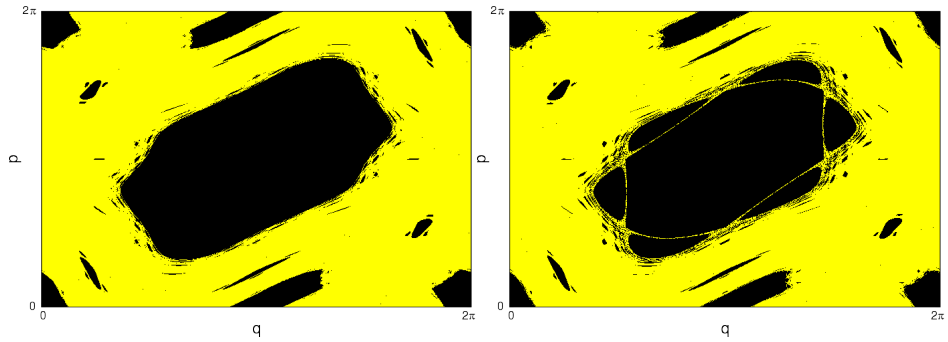

(a) $k = 1.45$ (b) $k = 1.46$

Figure 4.7: Separation the sea of chaos, yellow color, from the regular islands, black color, in the Standard mapping for two values of the nonlinear parameter. Smaller islands are ejected from the main island when we change the parameter value

We see in figure 4.7 the transition marked in figure 4.6. When passing from $k = 1.45$ to $k = 1.46$ the main island ejects a resonance of smaller islands, this reduces the area of the main island, but also each ejected island has an elliptic periodic point in the middle, and by the Poincaré Birkhoff theorem [52, 53] there exists their corresponding hyperbolic fixed points pair. The action of the stable and unstable manifolds of these hyperbolic points is responsible for the changes in diffusion behaviour since they provide *big channels* to escape from the main island [54, 55, 56].

Even with a more complicated mapping, the Oval Billiard, eq. (2.8), shows similar results, see figures 4.8 and 4.9. With these results we observe that changes of behaviour in the diffusion exponent are related with changes in the area of the main island. Particularly, we find that when the main island's area is abruptly reduced, due the destruction of invariant tori and creation of hyperbolic and elliptic fixed points, the diffusion exponent grows.

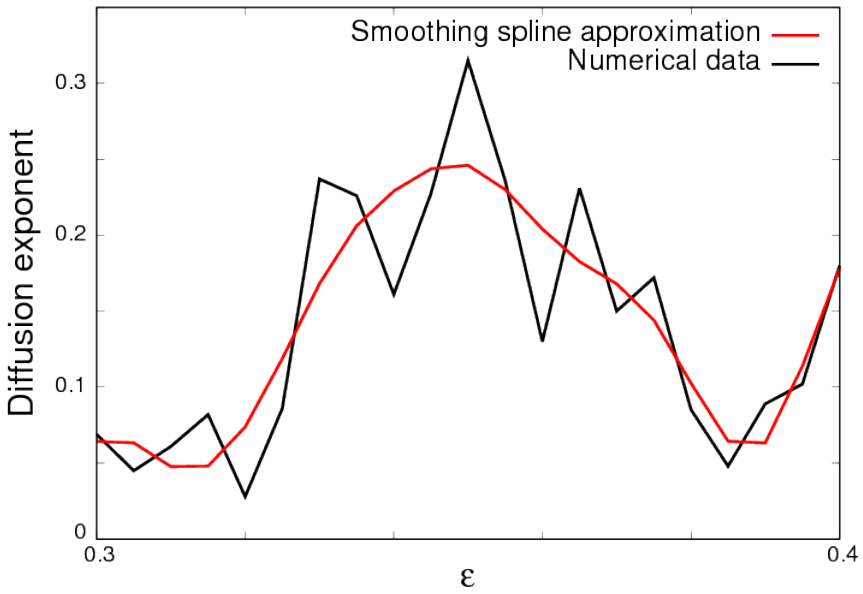

Figure 4.8: Plot of the Diffusion exponent vs. parameter ε of Oval Billiard. The black line represents the numerical data obtained after the power law fitting and the red line is an quintic spline smoothing approximation to the numerical data.

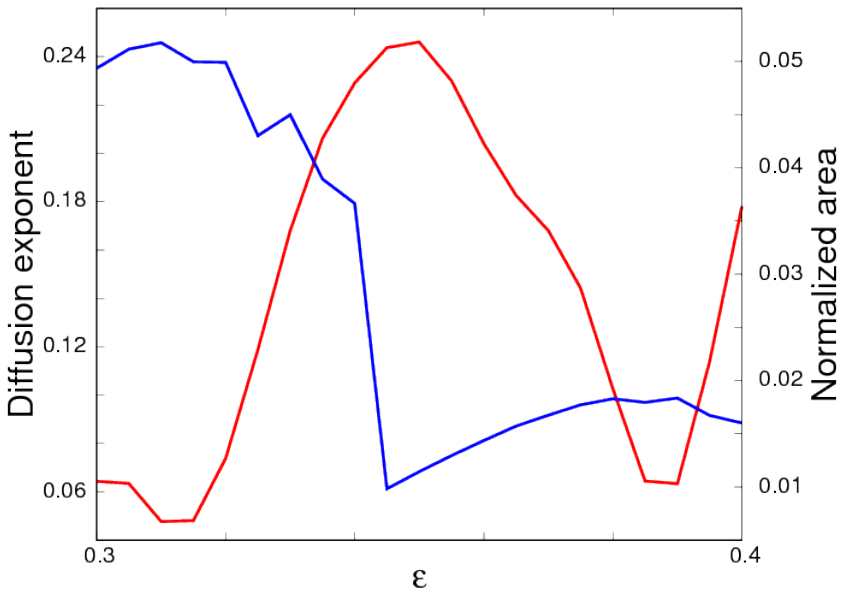

Figure 4.9: Plot of the diffusion exponent, red line, and normalized area of the main island, blue line vs. parameter ε of Oval Billiard. The normalized area is the area of the main island divided by the the area of the entire phase space.

4.4 Controlling escape, a targeting algorithm

To study the influence of the hyperbolic fixed point in the diffusion dynamic, we perform an appropriate control scheme in the Standard Map. The idea is target to initial conditions that do not escape of the island's shore by a given control area, and characterize they diffusion behaviour, with this we can evaluate the importance of the control area in the escape of trajectories. The targeting algorithm consists in the following steps:

1. Choose a two dimensional I (horizontal divisions) $\times J$ (vertical divisions) grid with help of the relation $10 \times \frac{diffusion\ \ range}{fluctuation\ \ size} \sim grid\ \ divisions$, Eq (3.8).

2. Set an ensemble of initial conditions around the KAM island to apply the mapping.

3. Choose a control area in phase space [4].

4. Apply the mapping (4.1) to the ensemble of orbits. At each iteration construct an histogram $[h_{ij}]$ counting how many points are inside each grid box. Then measure the entropy by means of the equation $S = -\sum_{i=1}^{I}\sum_{j=1}^{I} h_{ij}\ln(h_{ij})$, Eq. (3.7).

5. At every iteration for each element of the ensemble of orbits ask if the orbit has entered in the control area. If it does it, re-initiate the orbit choosing a new initial condition randomly from our ensemble of orbits at $n = 0$, i. e. we target to initial conditions that do not pass in the control area.

6. After some iterations search of a interval in time where the entropy grows linearly[5] with $\ln(n)$.

7. Use the equation $S = A + \delta\ln(n)$, Eq. (3.6), to calculate the diffusion exponent δ.

For a given value of k in the SM, Eq. (4.1), we search the hyperbolic points, associated to the smaller islands ejected, and control a circular area around them when we calculate the diffusion exponent. Then we change the control's area, and position. With

[4] In our case an circular ball of some radius.

[5] In this region is possible to consider the scaling hypothesis of [30].

this we can observe the influence of the given fixed hyperbolic point in the diffusion dynamic.

k	Period	δ (with control)	δ (no control)
1.46	6	0.143 ± 0.001	0.247 ± 0.001
1.47	6	0.2448 ± 0.0009	0.3218 ± 0.0009
1.48	6	0.152 ± 0.003	0.288 ± 0.003
1.96	10	0.201 ± 0.009	0.221 ± 0.009
1.97	10	0.25 ± 0.01	0.275 ± 0.009
1.98	10	0.179 ± 0.007	0.189 ± 0.007

Table 4.1: Table showing changes in the diffusion exponent when controlling an small circular area around hyperbolic points, (ball radius $r = 0.001$) .

In table 4.1 we show the effect of the control scheme in the standard map. The first column is the value of the Standard Map's parameter k. Second column gives the period of the hyperbolic fixed point analyzed. Third and fourth column show the values of the diffusion exponent with and without control respectively. We can appreciate the change in diffusion exponent when an area around the hyperbolic points is controlled. For different values of the parameter k we have different periods in the resonance islands, but in every case the diffusion exponent becomes smaller than without the control. The values of k were chosen near two decays in the normalized area from figure 4.6.

We examine now the effect of the control area, we change the radius of the circular ball around the hyperbolic fixed points and see how does the diffusion exponent changes, see figure 4.10.

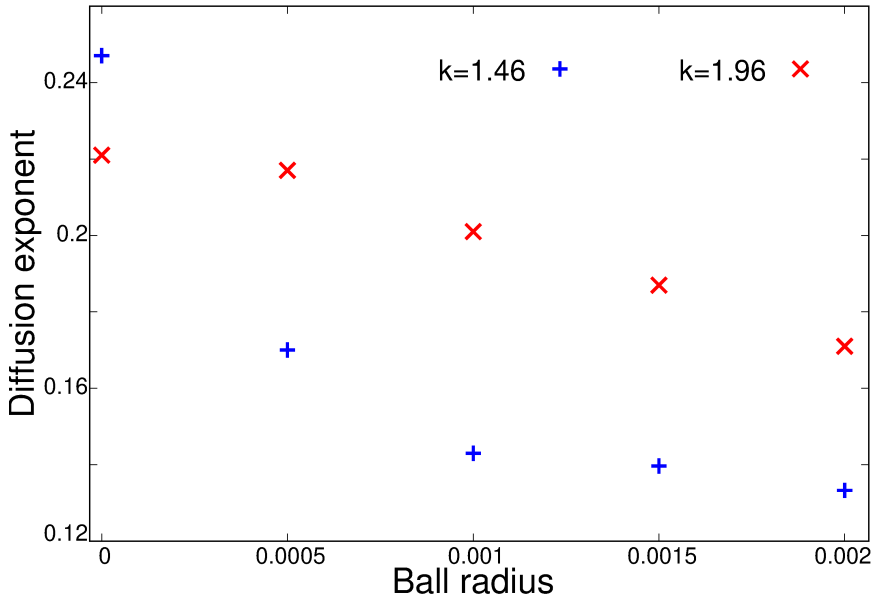

Figure 4.10: Plot of the diffusion exponent against the radius of the controlling ball for two values of the control parameter, namely $k = 1.46$ and $k = 1.96$.

It is possible to see in figure 4.10 that a bigger value radius of control area, horizontal axis, translates into a smaller value of the diffusion exponent, vertical axis. This has a direct explanation, when the ball radius grows, it is more likely than a orbit enters in the control area, this translates in more orbits being re-initiated, then, the ensemble of trajectories diffuses more slowly.

Haven seen the action of the control area around the hyperbolic fixed point, we examine the action of placing the control at random points in phase space and compare them against our first results with control.

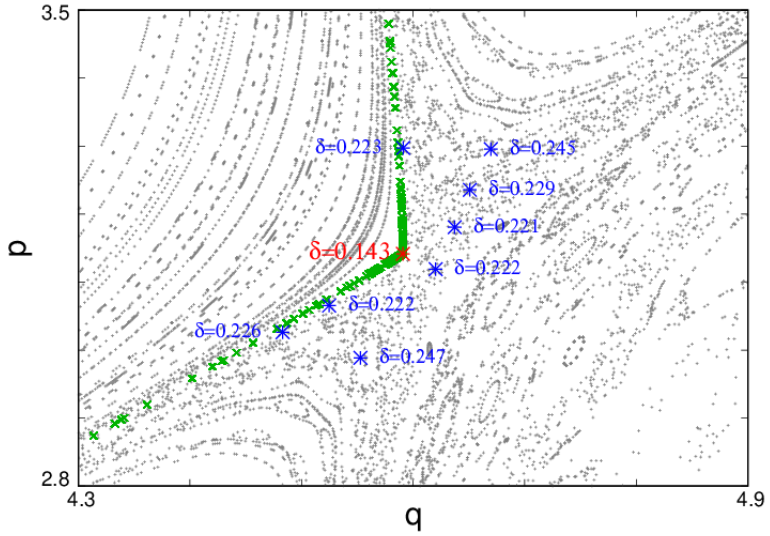

Figure 4.11: Plot of diffusion exponent for $k = 1.46$, the position of the control point is indicated with blue points with its diffusion exponent next to them. The red point indicates the hyperbolic fixed point. The green points are the initial ensemble of conditions. The gray dots in the background shows the Standard Map portrait for that value of k.

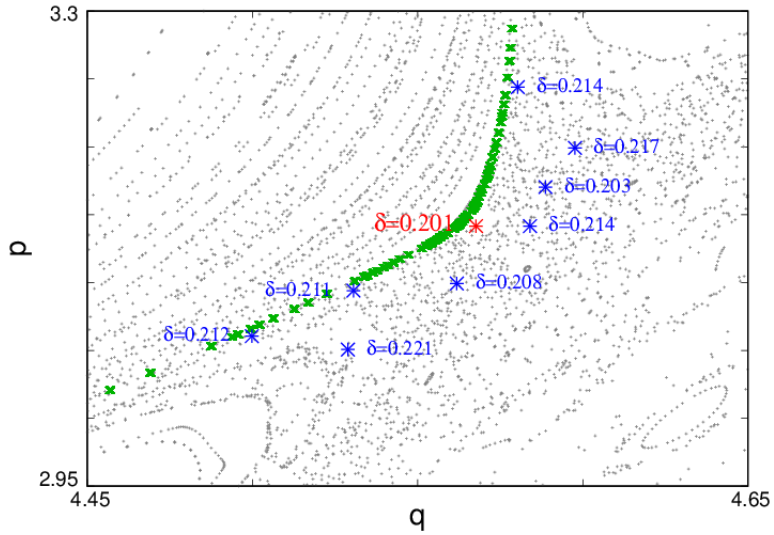

Figure 4.12: Plot of the diffusion exponent for $k = 1.96$, the position of the control point is indicated with blue points with its diffusion exponent next to them. The red point indicates the hyperbolic fixed point. The green points are the initial ensemble of conditions. The gray dots in the background shows the Standard Map portrait for that value of k.

When we change the position of the control area, the diffusion exponent also changes, as can be seen in figures 4.11 and 4.12. We notice the diffusion exponent seems to be more affected when the control area is around an hyperbolic point (red point) than when is around another random point (blue points).

4.5 The manifold effect

From the hyperbolic fixed point we change the focus of our attention to the unstable manifold, and study its effect in the diffusion dynamic.

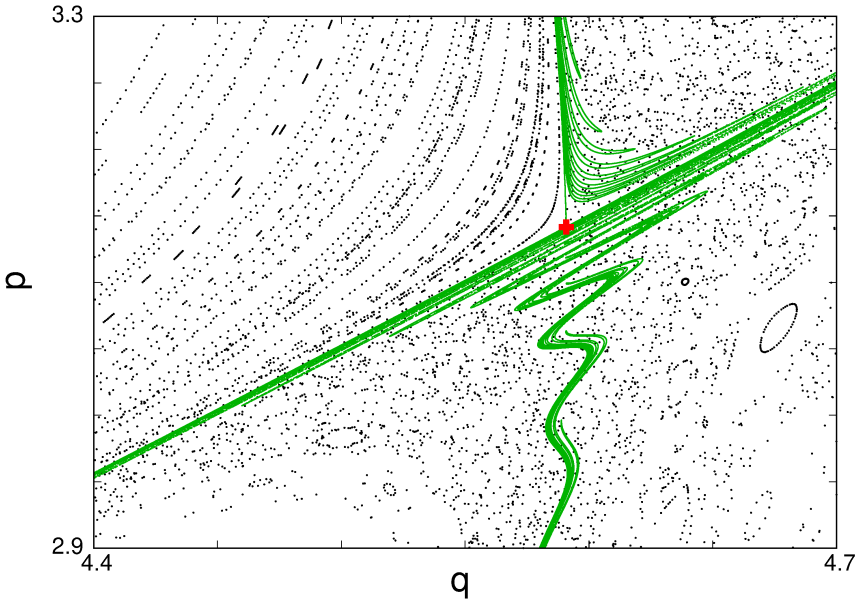

Figure 4.13: Phase space portrait of Standard Map for $k = 1.46$. The green points are the unstable manifold associated to the hyperbolic fixed point of period 6, red point.

In figure 4.13 we show the unstable manifold, green points, for the period 6 hyperbolic fixed point, red point, the mapping is the SM with $k = 1.46$. It is possible to appreciate that near the fixed point the manifold has a lot o zig-zags. Since trajectories tend to align along the unstable manifold, we expect that regions near it have a lot visitations from an ensemble of trajectories.

For the initial ensemble of conditions, green points shown in figure 4.11, we calculate the number of times any of them enters a small box of a grid when we perform

iterations of the SM. According to the number of times any point entered, a box is assigned with a given color, see figure 4.14.

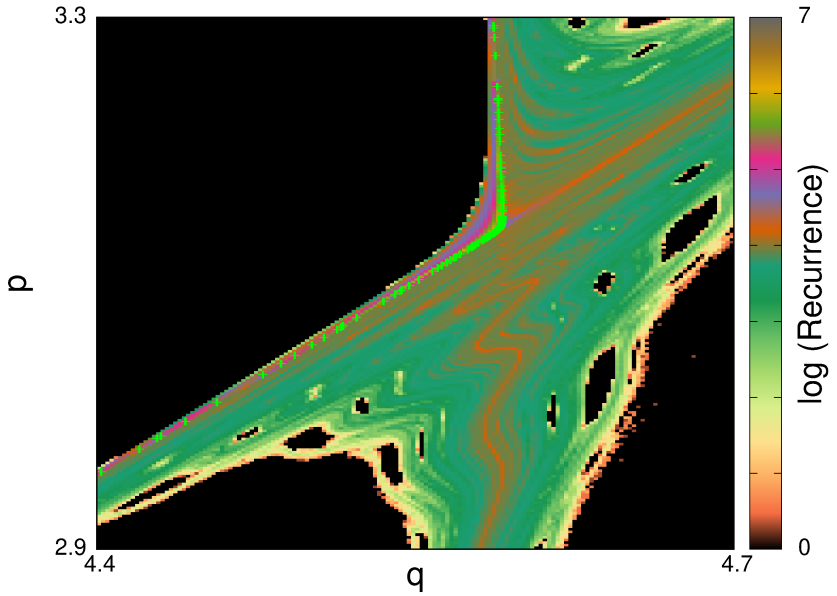

Figure 4.14: Recurrence plot for the initial ensemble of orbits (green points). Every box in the grid has a color assigned depending on the number of points visited them, see the color box.

It is possible to see in figure 4.14 that the manifolds zig-zag is still visible in the recurrence plot, meaning that indeed regions near the unstable manifold are highly visited. Since trajectories are common to be found in this regions we expect them to be good places to perform the control in the SM iterations, method discussed in last section. See figure 4.15

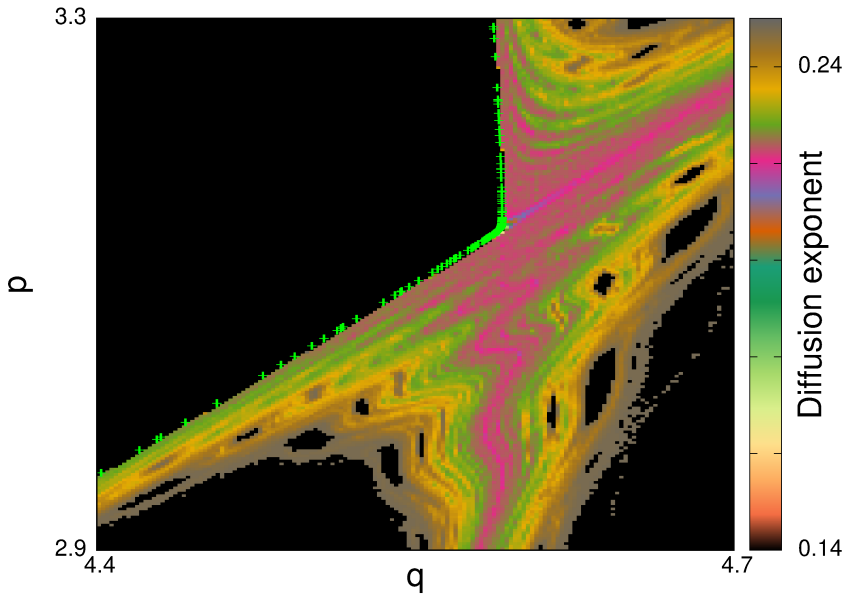

Figure 4.15: Diffusion exponent for the initial ensemble of orbits (green points). Every box in the grid has a color assigned depending on the value of the diffusion exponent when the control area is in the grid box.

In figure 4.15 wee see a color grid with the value of the diffusion exponent when the control area is in each grid box. We notice the diffusion exponent near the hyperbolic point is smaller than in other regions. Even more, this figure shows similar zig-zag structure as seen in figures 4.14 and 4.15. This means that the unstable manifold creates small channels were the control is better than away from those channels.

Further on our study of the manifold effect, we care about the entropy growth behaviour. We perform several simulations. For each simulation we start with a given number of points over the unstable manifold, see table 4.2, then, we add noise to these points until we have an ensemble of 1×10^8 initial conditions, using this ensemble we start iterating the SM and study the ensemble's entropy growth.

	Points in manifold
Simulation 1	1720594
Simulation 2	0
Simulation 3	720594
Simulation 4	20594

Table 4.2: Table showing the number of starting points in the unstable manifold for each simulation. The rest of the points are noise added in the manifold until we reach an ensemble of 1×10^8 initial conditions .

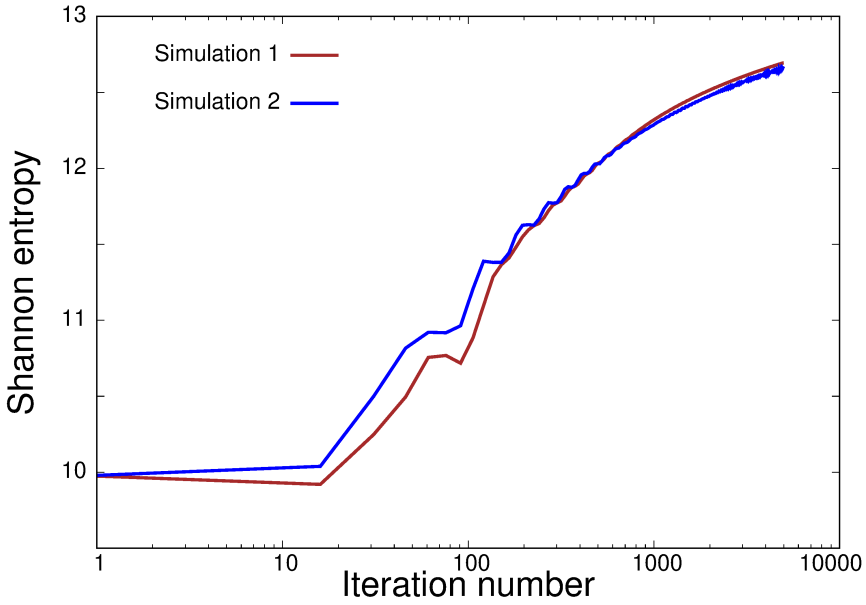

Figure 4.16: Entropy growth for different number of initial conditions over the unstable manifold. Simulation 1, brown line, and Simulation 2, blue line, are described in Table 4.2.

Figure 4.16 shows the entropy growth for Simulation 1, whose initial ensemble has several points over the manifold, and Simulation 2, whose initial ensemble are noisy random points near the manifold. We observe that for small number of iterations Simulation 2 is over Simulation 1, this is expected due the initial noise, until some iteration when Simulation 1 surpass Simulation 2, this due the fact that, having more points over the unstable manifold, they escape more rapidly to other regions. We can also observe that Simulation 2 is aligning to Simulation 1.

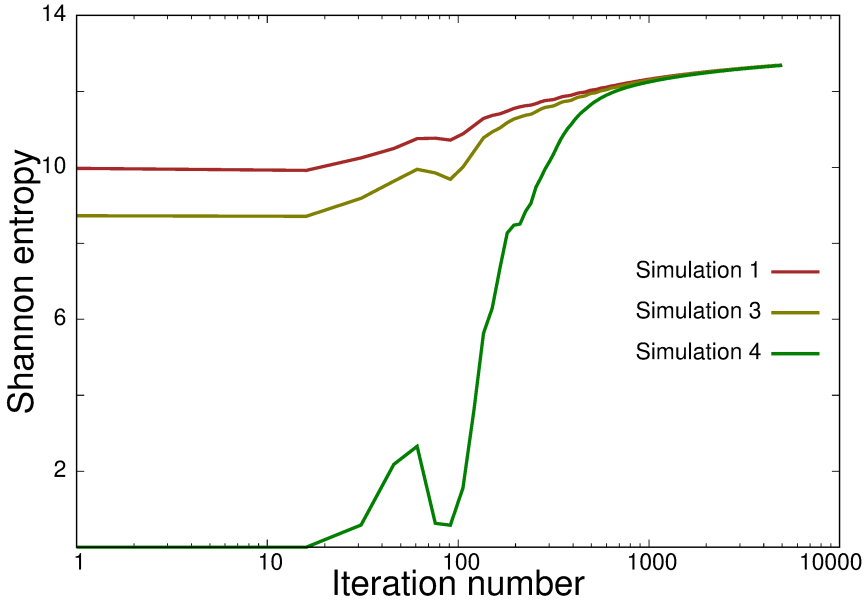

Figure 4.17: Entropy growth for different number of initial conditions over the unstable manifold. Simulation 1, brown line, and Simulation 3, light green line, and Simulation 4, green line, are described in Table 4.2.We see that all converge to the same entropy behaviour after some number of iterations.

In figure 4.17 we can see the entropy growth for Simulations 1, 3 and 4. It is clear that initially each one has its own entropy. Simulation 1 having the biggest initial entropy since their 1720594 initial points are distributed over a bigger number of grid boxes, Simulation 4 has the lower entropy, zero, since initially all its points are in just one grid box, and Simulation 2 a medium entropy value. When the iterations start, we can see that Simulation 4 grows very rapidly until it aligns with Simulation 1, this means that in the first iterations the points of Simulation 4 go through a superdiffusive behaviour until the ensemble is distributed on phase space almost as Simulation 1. From there both Simulations behave similarly. Same happens with Simulation 3. From this behaviour we conjecture that there exists a biggest entropy growth curve given when all the ensemble points over the unstable manifold, even more, this entropy curve is the limit behaviour of all the other possible entropy growth for ensembles running away from the sticky effect of the main island plus resonances.

Chapter 5

Conclusions

We showed that the use of Shannon Entropy permits us to characterize the diffusion exponent in low dimensional Hamiltonian systems described by maps. The methodology proposed allowed us to calculate the diffusion exponent both in regions where the diffusion is normal, as in regions where the stickiness phenomenon is present, producing an anomalous diffusion.

We calculated the diffusion exponent for many values of the nonlinear parameter of the Standard Map and the Oval Billiard, where for each value the main island had a different shape, then we showed that the changes of behaviour in the diffusion exponent were related with changes in the area of the main island. Particularly, we found that when the main island's area is abruptly reduced, due the destruction of invariant tori and creation of hyperbolic and elliptic fixed points, the diffusion exponent grew.

To investigate the dependence of the diffusion exponent with the creation of resonance islands, we developed an appropriate control scheme in the Standard Map. Then, for different values of the nonlinear parameter k, where resonance islands were created, we showed that when considering an small control area, around hyperbolic points associated to the resonances, it is possible to change the diffusion exponent making it smaller. This is mainly due to the fact that the control action closes paths to escape from the main island. We also showed that the bigger the control area the smaller the diffusion exponent, since it is more probable that an orbit will enter the control area.

We showed that changing the position of the control point the diffusion exponent changes, for random control points this diffusion exponent is not much affected as when

we consider the hyperbolic point. Then, by performing a detailed analysis in phase space of the relation position of control point Vs Diffusion exponent, and comparing this with the portrait of the unstable manifold, we showed that this manifold provides small channels for the escape of trajectories from the main island.

Finally, observing the entropy's behaviour of different ensembles of trajectories, and watching the alignment tendency of the entropy curves, we conjectured that there exists a biggest entropy growth curve given when all the ensemble points are over the unstable manifold, even more, this entropy curve is the limit behaviour of all the other possible entropy growths for ensembles running away from the sticky effect of the main island plus resonances.

Chapter 6

Perspectives

Even though the Standard Map is a prototypical example for Hamiltonian Systems, it would be interesting to explore and confirm the results in other systems, in this work we expanded some results to the Oval Billiard and showed that behave similarly as in the Standard Map, this encourages to extend the methodology to other Hamiltonian Systems. In the case of higher dimensional Hamiltonian Systems the invariant structures presented in phase space are different, in principle is possible to extend the DEA method to these systems, although constructing frequency histograms for high dimensional spaces becomes more challenging, so a possible way to overcome this could be to project to lower dimensional spaces and use cumulative probability distribution functions, and see if it is possible to calculate diffusion exponents.

Another point of interest is the manifold's effect of other resonance islands, here we had our focus in the first resonance island, although it is known that the hyperbolic point's manifolds extend all over phase space, meaning that is not a localized effect, it is also known that other hyperbolic point's manifolds also exist and affect the dynamics. So, it would be interesting to study what happens with the entropy behaviour for ensembles near the crossing points of the manifolds, it can be expected that these regions present interesting dynamics since they go easily from one resonance to another, this could facilitate the diffusion, or on the contrary, make the trajectories enter even more in sticky regions.

Appendix A

For those about to map

In this appendix we describe the maps used in this thesis.

A.1 Standard Map

The Standard Map is constructed by a Poincaré section of the kicked rotator, which describes the motion of a particle constrained to move in a ring. The particle is kicked periodically by an external field. The model is described by the Hamiltonian

$$H\left(q,p,t\right) \;=\; \frac{p^2}{2mr^2} + K\cos\left(q\right)\sum_{n=-\infty}^{\infty}\delta\left(t/T-n\right), \tag{A.1}$$

where δ is the Dirac delta function, q is the angular coordinate and p is its conjugate momentum. It is worth remarking that we can consider that the particle's mass m, the ring's radius r and the period of kicks T are equal to one, this due the fact that we have three unit dimensions, length, time and energy (or mass). For now we will leave the additional parameters until the final steps.

Now we make use of Hamilton's equations of motion

$$\begin{aligned} \dot{p} \;=\; -\frac{\partial H}{\partial q} \;&=\; K\sin\left(q\right)\sum_{n=-\infty}^{\infty}\delta\left(t/T-n\right), \\ \dot{q} \;=\; \frac{\partial H}{\partial p} \;&=\; \frac{p}{mr^2}. \end{aligned} \tag{A.2}$$

We will analyze the movement in the interval of time just before the kick at $t = 0$ and the kick at $t = T$, i. e. $t \in [-\epsilon, T - \epsilon]$. For other intervals of time the analysis would be similar due the periodicity of the kicks.

From Hamilton's equations A.2 we can see that the instant of the kick in $t = 0$ the momentum has an abrupt change and then remains constant

$$\begin{aligned} \int_{-\epsilon}^{T-\epsilon} \dot{p}\, dt &= \int_{-\epsilon}^{T-\epsilon} K \sin(q) \sum_{n=-\infty}^{\infty} \delta(t/T - n)\, dt, \\ p - p_0 &= KT \sin(q). \end{aligned} \tag{A.3}$$

After the kick at $t = 0$ the movement is uniform so the change in coordinate is given by:

$$\begin{aligned} \int_{-\epsilon}^{T-\epsilon} \dot{q}\, dt &= \int_{-\epsilon}^{T-\epsilon} \frac{p}{mr^2}\, dt, \\ q - q_0 &= \frac{p}{mr^2} T. \end{aligned} \tag{A.4}$$

Finally, rescaling the momentum $\frac{pT}{mr^2} \to p$, and generalizing for any kick, we arrive to:

$$\begin{aligned} p_{n+1} &= p_n + \frac{KT^2}{mr^2} \sin(q_n), \\ q_{n+1} &= q_n + p_{n+1}. \end{aligned} \tag{A.5}$$

Which is the Standard Map if we consider $k = \frac{KT^2}{mr^2 l}$. This map is area preserving, the Jacobian of the transformation $(q_{n+1}, p_{n+1}) = M(q_n, p_n)$ is given by

$$\frac{\partial(q_{n+1}, p_{n+1})}{\partial(q_n, p_n)} = \begin{pmatrix} \frac{\partial q_{n+1}}{\partial q_n} & \frac{\partial q_{n+1}}{\partial p_n} \\ \frac{\partial p_{n+1}}{\partial q_n} & \frac{\partial p_{n+1}}{\partial p_n} \end{pmatrix} = \begin{pmatrix} 1 + k\cos(q_n) & 1 \\ k\cos(q_n) & 1 \end{pmatrix}, \tag{A.6}$$

and it's determinant is 1:

$$\left\| \frac{\partial(q_{n+1}, p_{n+1})}{\partial(q_n, p_n)} \right\| = \begin{Vmatrix} 1 + k\cos(q_n) & 1 \\ k\cos(q_n) & 1 \end{Vmatrix} = 1, \tag{A.7}$$

This means that the mapping is area preserving since:

$$dq_n dp_n = \left| \left(\left\| \frac{\partial \left(q_{n+1}, p_{n+1} \right)}{\partial \left(q_n, p_n \right)} \right\| \right)^{-1} \right| dq_{n+1} dp_{n+1} \quad = \quad dq_{n+1} dp_{n+1}. \qquad \text{(A.8)}$$

A.2 Simplified Fermi Ulam Model

The Simplified Fermi Ulam Model consists of a classical particle going through elastic collisions in a confined region bounded by two walls, separated by a distance equal to l, one of the walls is fixed and the other capable of exchange energy with the particle, affecting the particle's velocity depending on which phase of movement is the wall, see figure A.1. The model has two unit dimensions, length and time, so we can choose that the distance between the walls and the period of the walls phase change are equal to one. We will leave the additional parameters until the final step.

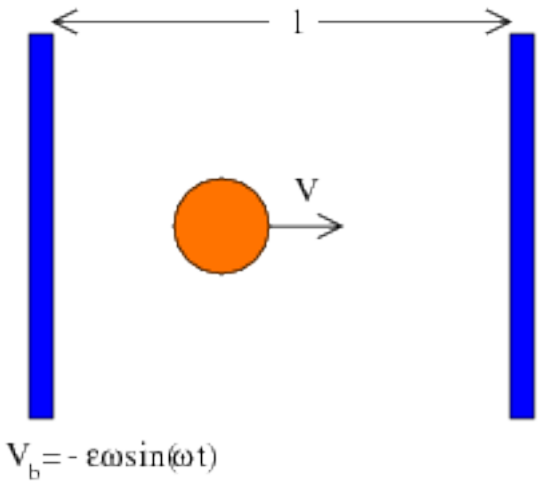

Figure A.1: The Simplified Fermi Ulam Model, a particle bounces between two walls separated by a distance equal to l. One of the walls acts as if it moves when the particle collides with it, the wall's velocity is $V_b = -\varepsilon\omega \sin(\omega t)$

Since the movement between collisions is of a free particle, and the collision with

the right wall is elastic and the wall is not moving, we will care about collision with the left wall. The time between the n^{th} collision and the next one is given by:

$$t_{n+1} - t_n = \frac{2l}{V_n}. \tag{A.9}$$

where we considered that the particle's velocity after the n^{th} collision is V_n. Which is the same magnitude, but different direction, as the particle's velocity just before the next collision. For the collision we consider the left wall as if it were moving, with velocity $-\varepsilon\omega\sin(\omega t_{n+1})$, then the particle's velocity, relative to the wall, just before the collision, V_n', is the same as the particle's velocity, relative to the wall, just after the the collision, V_{n+1}', but with different sign, elastic collision. We have the following equations:

$$V_n' = -V_n + \varepsilon\omega\sin(\omega t_{n+1}), \tag{A.10}$$
$$V_{n+1}' = V_{n+1} + \varepsilon\omega\sin(\omega t_{n+1}), \tag{A.11}$$
$$V_n' = -V_{n+1}'. \tag{A.12}$$

Finally, making the following change of variables $\omega t \to \phi$, $\frac{V}{\varepsilon\omega} \to V$ and $\frac{\varepsilon}{l} \to \epsilon$ we arrive to the Simplified Fermi Ulam Model:

$$\begin{aligned} \phi_{n+1} &= \left[\phi_n + \frac{2}{V_n}\right] \mod (2\pi), \\ V_{n+1} &= \|V_n - 2\epsilon\sin(\phi_{n+1})\|. \end{aligned} \tag{A.13}$$

Note that in this case the Jacobian of the transformation is:

$$\frac{\partial(\phi_{n+1}, V_{n+1})}{\partial(\phi_n, V_n)} = \begin{pmatrix} 1 & -\frac{2}{V_n^2} \\ -2\epsilon\cos(\phi_{n+1})\,\mathrm{sgn}(V_{n+1}) & \left(1 + 2\epsilon\cos(\phi_{n+1})\frac{2}{V_n^2}\right)\mathrm{sgn}(V_{n+1}) \end{pmatrix} \tag{A.14}$$

where $\mathrm{sgn}(V_{n+1})$ is the sign function, takes the value 1 if $V_{n+1} > 0$ and -1 if $V_{n+1} < 0$. It's determinant is:

$$\left\|\frac{\partial(\phi_{n+1}, V_{n+1})}{\partial(\phi_n, V_n)}\right\| = \mathrm{sgn}(V_{n+1}). \tag{A.15}$$

Then this map is area preserving:

$$d\phi_n dV_n = d\phi_{n+1} dV_{n+1}. \tag{A.16}$$

A.3 Oval Billiard

The Oval Billiard consists in a free moving particle; whose position is given by:

$$\begin{aligned} x - x_0 &= v_{x0} t \, , \\ y - y_0 &= v_{y0} t \, , \end{aligned} \tag{A.17}$$

inside a closed region whose boundary radius[1] is written as:

$$R\left(\theta, \epsilon, p\right) = 1 + \varepsilon \cos\left(p\theta\right) \, , \tag{A.18}$$

where the parameter $\varepsilon \in [0, 1)$ controls the deformation of the circle, the non linearity, p is an integer number and $\theta \in [0, 2\pi)$ is the polar angle. Every time that the particle reaches the border suffers from a elastic collision, see figure A.2.

[1] Using polar coordinates.

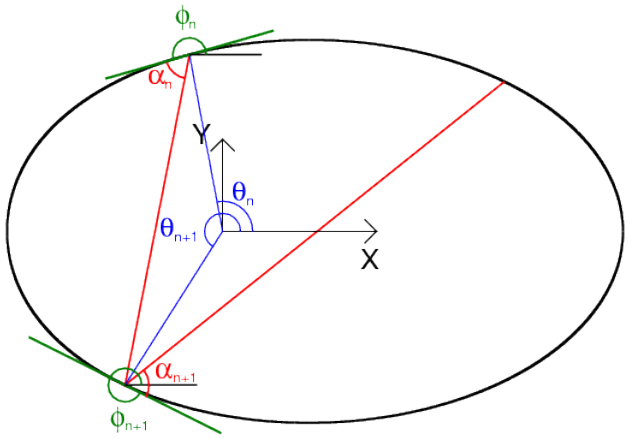

Figure A.2: Trajectory of a particle inside an oval billiard with $p = 1$ and $\varepsilon = 0.3$

After each collision of the particle with the wall we write two variables, the angle θ of collision, and the angle α that makes the trajectory with the tangent to the boundary, since we consider elastic collisions the velocity component tangent to the boundary is conserved while the normal component changes sign. From this we get the relation:

$$\alpha_{n+1} = \phi_{n+1} - (\alpha_n + \phi_n) , \tag{A.19}$$

where the auxiliar angle ϕ is the angle between the X axis and the line tangent to the boundary at the collision point.

The particle's energy is conserved both during the free flight as during the collision, so for simplicity we can consider that the modulus of the velocity is 1. The movement from the n^{th} collision to the next collision is described by:

$$\begin{aligned} x_{n+1} - x_n &= \cos(\phi_n + \alpha_n)\, t , \\ y_{n+1} - y_n &= \sin(\phi_n + \alpha_n)\, t . \end{aligned} \tag{A.20}$$

Call s the boundary's arc-length. Then the following relations hold over the boundary

[41]:

$$dx = \cos(\phi)\, ds\,, \tag{A.21}$$

$$dy = \sin(\phi)\, ds\,, \tag{A.22}$$

$$d\phi = -\kappa ds\,, \tag{A.23}$$

where κ is the boundary's curvature. Differentiating eqs. (A.19) and (A.20) we get:

$$\begin{aligned} d\alpha_{n+1} + \kappa_{n+1} ds_{n+1} &= \kappa_n ds_n - d\alpha_n\,, \\ \cos(\phi_{n+1})\, ds_{n+1} - \cos(\phi_n)\, ds_n &= \cos(\phi_n + \alpha_n)\, dt - t \sin(\phi_n + \alpha_n)\,(d\phi_n + d\alpha_n)\,, \\ \sin(\phi_{n+1})\, ds_{n+1} - \sin(\phi_n)\, ds_n &= \sin(\phi_n + \alpha_n)\, dt + t \cos(\phi_n + \alpha_n)\,(d\phi_n + d\alpha_n)\,, \end{aligned} \tag{A.24}$$

After some algebraic manipulations we find:

$$\frac{\partial(s_{n+1}, \alpha_{n+1})}{\partial(s_n, \alpha_n)} = \frac{1}{\sin(\alpha_{n+1})} \begin{pmatrix} \sin(\alpha_n) + t\kappa_n & -t \\ \kappa_n \sin(\alpha_{n+1}) - \kappa_{n+1} \sin(\alpha_n) - t\kappa_n\kappa_{n+1} & t\kappa_{n+1} - \sin(\alpha_{n+1}) \end{pmatrix} \tag{A.25}$$

The determinant is:

$$\left\| \frac{\partial(s_{n+1}, \alpha_{n+1})}{\partial(s_n, \alpha_n)} \right\| = -\frac{\sin(\alpha_n)}{\sin(\alpha_{n+1})}. \tag{A.26}$$

Then this map preserves the area:

$$ds_n\, d\cos(\alpha_n) = ds_{n+1}\, d\cos(\alpha_{n+1})\,, \tag{A.27}$$

where we recognize the tangential velocity $v_n = \cos(\alpha_n)$. Thus the Oval Billiard is area preserving considering the Poincaré-Birkhoff coordinates, i. e. arch-length and tangential velocity.

Appendix B

Oval Billiard, an algorithm to solve it

In the oval billiard the radius of the boundary, in polar coordinates, is given by:

$$R_b(\theta) = 1 + \varepsilon \cos(p\theta). \tag{B.1}$$

If we know the position (x_0, y_0) and velocity (v_{x0}, v_{y0}) of the particle immediately after a collision, iteration 0, we want to know the position (x_1, y_1) and the velocity (v_{x1}, v_{y1}) of the particle after the next collision, iteration 1.

For the case of $p = 1$ a very simple algorithm exist to find exact solution. Let us rewrite the boundary radius in the following way:

$$R_b = 1 + \varepsilon \frac{x_1}{R_b}, \tag{B.2}$$

where R_b is the radius of the boundary in collision 1. Since the particle moves freely between collisions we know that $x_1 = x_0 + v_{x0}t$, t is the time from collision 0 to collision 1. After doing some algebra with equation (B.2) we arrive to:

$$R_b^2 = \left(R_b^2 - \varepsilon (x_0 + v_{x0}t)\right)^2. \tag{B.3}$$

Then we use the following auxiliar variables $A = x_0^2 + y_0^2$, $B = 2(x_0 v_{x0} + y_0 v_{y0})$ and $C = v_{x0}^2 + v_{y0}^2$ and the fact that $R_b^2 = (x_0^2 + v_{x0}t)^2 + (y_0^2 + v_{y0}t)^2$ in equation (B.3)

to find:

$$\begin{aligned} &\left(-A + A^2 - 2A\varepsilon x_0 + \varepsilon^2 x_0^2\right) \\ &+ \left(-B + 2AB - 2B\varepsilon x_0 - 2\varepsilon A v_{x0} + 2\varepsilon^2 x_0 v_{x0}\right) t \\ &+ \left(B^2 - C + 2AC - 2C\varepsilon x_0 + \varepsilon^2 v_{x0} - 2\varepsilon B v_{x0}\right) t^2 \\ &+ \left(2BC - 2\varepsilon C v_{x0}\right) t^3 + Ct^4 \quad = \quad 0. \end{aligned} \tag{B.4}$$

The first term is zero since the initial position is in the boundary, then we have to solve a third degree polynomial, which has exact solution [47]. We use the algorithm written by Skowron and Gould [46] to find the roots of the polynomial, then we pick the smallest real root bigger than zero, this is our time between collision 0 and 1. With this we can find the collision angle θ_1.

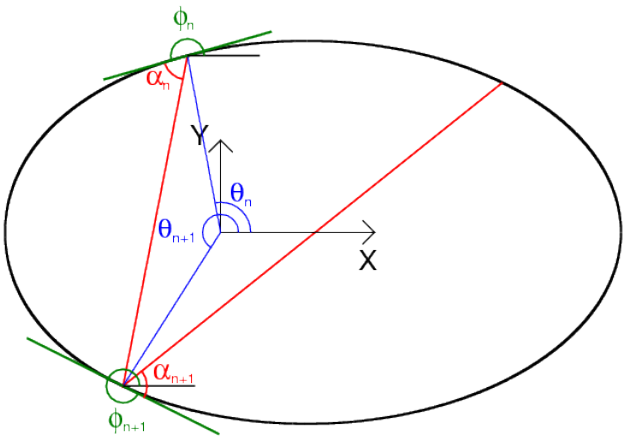

Figure B.1: Trajectory of a particle inside a oval billiard with $p = 1$ and $\varepsilon = 0.3$

We are interested now in the angle α_{n+1}, by means of figure B.1 we find the relation:

$$\alpha_{n+1} \quad = \quad \phi_{n+1} - (\alpha_n + \phi_n)\,, \tag{B.5}$$

where the auxiliar angle ϕ is related to the tangent line to the boundary at the point of

collision, is the angle between the X axis and the tangent line, so it is given by:

$$\phi \;=\; \arctan\left(\frac{dY_b}{dX_b}\right), \tag{B.6}$$

using the chain rule and the parametric description of the boundary given by θ, we finally find that ϕ is:

$$\phi_n \;=\; \arctan\left(\frac{-p\varepsilon\sin\left(p\theta_n\right)\sin\left(\theta_n\right)+R\left(\theta_n\right)\cos\left(\theta_n\right)}{-p\varepsilon\sin\left(p\theta_n\right)\cos\left(\theta_n\right)-R\left(\theta_n\right)\sin\left(\theta_n\right)}\right). \tag{B.7}$$

Appendix C

A little more on diffusion

In this appendix we comment on anomalous diffusion, the reasons behind the scaling relation[1]:

$$\rho\left(x,t\right) \;=\; \frac{1}{t^{\delta}}F\left(\frac{x}{t^{\delta}}\right), \tag{C.1}$$

and its validity in our mappings.

C.1 Anomalous Diffusion

A diffusion process is characterized by the behaviour of the Mean Squared Displacement (MSD) [59], contrary to normal diffusion, in an anomalous diffusion process, the MSD does not grow linearly in time:

$$\left\langle x^{2}\left(t\right)\right\rangle \;\propto\; t^{\alpha};\;\; \alpha\neq 1 \tag{C.2}$$

where $\langle\cdot\rangle$ means ensemble average and we use the variable α instead of $\delta = \frac{\alpha}{2}$ for reasons that will become apparent later on. A subdiffusive process has $\alpha < 1$ and a superdiffusive one has $\alpha > 1$. Observe that in this equation two things are assumed, i) all the trajectories in the ensemble start in the position $x\left(0\right) = 0$, ii) the diffusion process happens in an infinity space.

[1] Equation (3.4) in the main text

First we use an heuristic approach to get relation (C.1) from equation (C.2), then we will use a more rigorous proof.

From Eq. (C.2) we can see that the $length$ scales with $time^{\alpha/2}$. Then, the differential probability $\rho\left(length, time\right) d(length)$ should behave like:

$$\rho\left(length, time\right) d(length) \quad = \quad \rho\left(\frac{length}{time^{\frac{\alpha}{2}}}\right) \frac{d(length)}{time^{\frac{\alpha}{2}}}, \tag{C.3}$$

in order to preserve the total probability. From las equation, the relation (C.1) easily follows.

There are different physical scenarios that lead to anomalous diffusion [59], among them, the most common scenarios are continuous time Random Walk (CTRW) [61] and Fractional Brownian Motion (FBM) [60]. Scaffeta and Grigolini [30] discussed scaling behaviour (C.1) in FBM and Lévy Flights. Even more, they showed in numerical experiments that the Diffusion Entropy Analysis (DEA) method provides the value of the anomalous diffusion exponent.

The physical scenario for the Standard Map usually is considered be similar to the Fractional Diffusion Equation (FDE) [62], which in turn is connected with CTRW models [63].

Random Walk and Continuous Time Random Walk can be simulated with the following set of equations

$$\begin{aligned} P_{\alpha}\left(\nu, t\right) &= \sum_{i=0}^{\nu} g_{\alpha}\left(i, t\right) \ , \\ dX_{\nu} &= \left(2D\right)^{\frac{1}{2}} dB_{\nu} \ , \end{aligned} \tag{C.4}$$

where ν is an *operational time*, for simplicity we assume it is a discrete variable [63] and t is the physical time. At the first equation, $g_{\alpha}\left(\nu, t\right)$ defines the probability to make ν steps up to time t, $P_{\alpha}\left(\nu, t\right)$ is a cumulative distribution function, it says the probability to make at most ν steps up to time t, α is an scaling parameter which we will discuss later. At the second equation we have X_{ν} as a position at operational time ν, D the diffusion coefficient and dB_{ν} the standard Brownian noise. Then the dynamics of X_{ν} is a Random Walk (RW) in the operational time ν. These equations describe two independent stochastic processes, the time evolution given by the first equation, and the jump given by the second equation, both of them related trough the operational time.

The trajectory $X(t)$, that arises from both processes of Eq. (C.4) is itself a subordinated stochastic process.

The scaling parameter $\alpha \in (0,1]$ enters in the relation

$$\nu \propto t^{\alpha}, \tag{C.5}$$

allowing a sub-linear dependence of ν with t. Since long time t can go with a small operational time ν, this behavior is responsible for sub-diffusive dynamics. In terms of Eq. (C.4) it means that we can wait long time, trap-time, t until a *jump* is taken by X_{ν}. This scenario is the so called Continuous Time Random Walk (CTRW) model.

The behavior of an ensemble of trajectories that follows RW can be described by a probability density function $\rho_{\nu}(x)$ and, its evolution in the operational time is given by [64]:

$$\rho_{\nu+1}(x) = \int_{-\infty}^{\infty} dx' f(x-x')\,\rho_{\nu}(x') \ , \tag{C.6}$$

meaning that the probability $\rho_{\nu+1}(x)$ to be at x at time $\nu+1$ is given by the probability $f(x-x')$ to jump from x' to x, times the probability $\rho_{\nu}(x')$ of being at x' at time ν, summed over all the possible values of x'.

Given that we have a Brownian noise model in Eq. (C.4), our *jump-probability-function* $f(x-x')$ is given by:

$$f(x-x') = \frac{1}{\sqrt{4\pi D}} e^{-\frac{(x-x')^2}{4D}} \ . \tag{C.7}$$

Considering now the analysis of a given function F in a Fourier space, $\hat{F}(k) = \mathcal{F}\{F(x);k\} = \int_{-\infty}^{\infty} e^{-ikx} F(x)\,dx$. Setting F as wish, Eq. (C.6) can be rewritten as

$$\hat{\rho}_{v+1}(k) = \hat{f}(k)\,\hat{\rho}_{v}(k) \ . \tag{C.8}$$

One can notice that Eq. (C.8) is a recurrence relation that can be solved if the initial distribution $\hat{\rho}_0(k)$ is known. Considering the following points:

i) An initial distribution $\rho_0(x) = \delta(x)$;

ii) The Fourier transform of Eq. (C.7) is $\hat{f}(k) = e^{-Dk^2}$;

iii) Assuming ν a continuous variable.

We have that:

$$\hat{\rho}\left(k,\nu\right) \;=\; e^{-Dk^2\nu}\,. \tag{C.9}$$

Now, to be able to change from the operational to the physical time we use

$$\rho\left(x,t\right) \;=\; \int_0^\infty d\nu\;\rho\left(x,\nu\right)g\left(\nu,t\right)\;. \tag{C.10}$$

Eq. (C.10) means that the probability $\rho\left(x,t\right)$ to be at x at time t is given by the probability $g\left(\nu,t\right)$ to take ν steps up to time t, times the probability $\rho\left(x,\nu\right)$ to be at x after ν steps, summed over all the possible number of steps ν. Moreover, if the relation between the operational time and the physical time is given by $g\left(\nu,t\right) = \delta\left(t-\nu\right)$, which reasonably means $\alpha = 1$ in the relation (C.5), then, using Eqs. (C.9), (C.10) and the Laplace transform $\tilde{F}\left(s\right) = \mathcal{L}\{F\left(t\right);s\} = \int_0^\infty e^{-st}F\left(t\right)dt$, we get:

$$\hat{\tilde{\rho}}\left(k,s\right) \;=\; \frac{1}{s+Dk^2}\,. \tag{C.11}$$

Remembering the initial condition $\rho\left(x,0\right)$ we can invert the Fourier-Laplace transform and finally arrive on:

$$\frac{\partial\rho\left(x,t\right)}{\partial t} \;=\; D\frac{\partial^2\rho\left(x,t\right)}{\partial x^2}\,, \tag{C.12}$$

which is the Diffusion Equation. Meaning that an ensemble of trajectories following a RW behaves like a probability distribution function from the diffusion equation, as expected.

Continuous Time Random Walk enters in play when we want to address the anomalous diffusion case, $\alpha \in (0,1)$. Magdziarz proposed in [65] to use an inverse α-stable subordinator for $g_\alpha\left(\nu,t\right)$. Setting $u_\alpha\left(t,\nu\right)$, as the probability distribution function (PDF) for a completely skewed α stable process, by the following Laplace transform:

$$\tilde{u}_\alpha\left(s,\nu\right) \;=\; e^{-\nu s^\alpha}\,, \tag{C.13}$$

it follows that:

$$\begin{aligned} \tilde{u}_\alpha(s,\nu+1) &= \tilde{u}_\alpha(s,\nu)\,\tilde{u}_\alpha(s,1)\ , \\ u_\alpha(t,\nu+1) &= \int_0^t d\tau\ u_\alpha(t-\tau,1)\,u_\alpha(\tau,\nu)\ . \end{aligned} \tag{C.14}$$

From Eq. (C.14), one can notice that if U_1 is a random sample from $u_\alpha(t,1)$, and U_ν a random sample from $u_\alpha(t,\nu)$, then, $U_{\nu+1} = U_1 + U_\nu$ is a random sample from $u_\alpha(t,\nu+1)$. With that, U_ν is a strictly increasing α-stable Lévy motion [66, 65]. Furthermore, looking at the Laplace transform of $u_\alpha(t,\nu)$, is possible to infer the following scaling relation:

$$u_\alpha(t,\nu) \;=\; \frac{1}{\nu^{1/\alpha}} u_\alpha\left(\frac{t}{\nu^{1/\alpha}}\right)\ . \tag{C.15}$$

Now, one can define a random variable S_t as:

$$S_t \;=\; \inf\{\nu : U_\nu > t\}\ . \tag{C.16}$$

Considering an analogous $g_\alpha(\nu,t)$ from Eq. (C.4) to be an inverse α-stable subordinator, implies that S_t must be a random sample from it. Then, from Eq. (C.16), we get that $P(S_t < \nu) = P(U_\nu \geq t)$ and, therefore

$$\begin{aligned} \int_0^\nu d\nu g_\alpha(\nu,t) &= 1 - \int_0^t dt\ u_\alpha(t,\nu) \\ g_\alpha(\nu,t) &= -\frac{\partial}{\partial\nu}\int_0^t dt\ u_\alpha(t,\nu) \\ &= \frac{t}{\alpha\nu^{1+1/\alpha}} u_\alpha\left(\frac{t}{\nu^{1/\alpha}}\right) \\ g_\alpha(\nu,t) &= \frac{t}{\alpha\nu} u_\alpha(t,\nu)\ . \end{aligned} \tag{C.17}$$

With Eq. (C.17) and the relation at C.9 we infer that, in this case, Eq. (C.10) is given

by:

$$\begin{aligned}
\hat{\rho}\left(k,t\right) &= \int_0^\infty d\nu\; e^{-Dk^2\nu}\frac{t}{\alpha\nu^{1+1/\alpha}}u_\alpha\left(\frac{t}{\nu^{1/\alpha}}\right) \\
\hat{\hat{\rho}}\left(k,s\right) &= \int_0^\infty d\nu\; e^{-Dk^2\nu}s^{\alpha-1}e^{-\nu s^\alpha} \\
\hat{\hat{\rho}}\left(k,s\right) &= \frac{s^{\alpha-1}}{s^\alpha+Dk^2}\,. \qquad \text{(C.18)}
\end{aligned}$$

Finally, inverting the Fourier-Laplace transform, we arrive on:

$$\frac{\partial^\alpha\rho\left(x,t\right)}{\partial t^\alpha} = D\frac{\partial^2\rho\left(x,t\right)}{\partial x^2}\,, \qquad \text{(C.19)}$$

which is the Fractional Diffusion Equation.

A couple of remarks are noted:

1. $\hat{\hat{\rho}}\left(0,s\right)=\frac{1}{s}$, then $\hat{\rho}\left(0,t\right)=1$, and the probability is conserved;

2. $-\left[\frac{\partial^2}{\partial k^2}\hat{\hat{\rho}}\left(k,s\right)\right]_{k=0}=\frac{2D}{s^{\alpha+1}}$, then $\left\langle x^2\left(t\right)\right\rangle=\frac{2Dt^\alpha}{\Gamma(1+\alpha)}$, recovering the expected mean square displacement behavior.

3. See that $\hat{\rho}\left(k,t\right)=E_\alpha\left(-Dt^\alpha k^2\right)$, where $E_\alpha\left(z\right)$ is the Mittag Leffler function [67]. Thus, recalling the scaling property of the Fourier Transform $\mathcal{F}^{-1}\{\hat{F}\left(ak\right);x\}=\frac{1}{\|a\|}F\left(\frac{x}{\|a\|}\right)$ we have the result $\rho\left(x,t\right)=\frac{1}{\sqrt{Dt^\alpha}}\phi\left(\frac{x}{\sqrt{Dt^\alpha}}\right)$, which recovers the scaling relation (C.1).

4. If the initial distribution is given by $\rho_0(x)=\delta(x-x_0)$ we only have to change the location $x\to x-x_0$ and all the demonstrations still hold.

It is important to mind that the analysis made from Eq. (C.13) to the FDE presented in Eq. (C.19) means that, an ensemble of trajectories following a CTRW-like model, behaves as a probability distribution function from the solution of the FDE.

Considering this analytical background of either normal and anomalous diffusion process, connected respectively to RW and CTRW, we use the set of equations in Eq. (C.4) and follow the numerical method proposed by Magdziarz in [65] to simulate the dynamics of a RW process, setting $\alpha=1$ and the CTRW process, setting $\alpha=0.6$

(relatively not so long trap-time) and $\alpha = 0.3$ (relatively long trap-time). In figure C.1 we show examples of simulated trajectories of these three different dynamic scenarios.

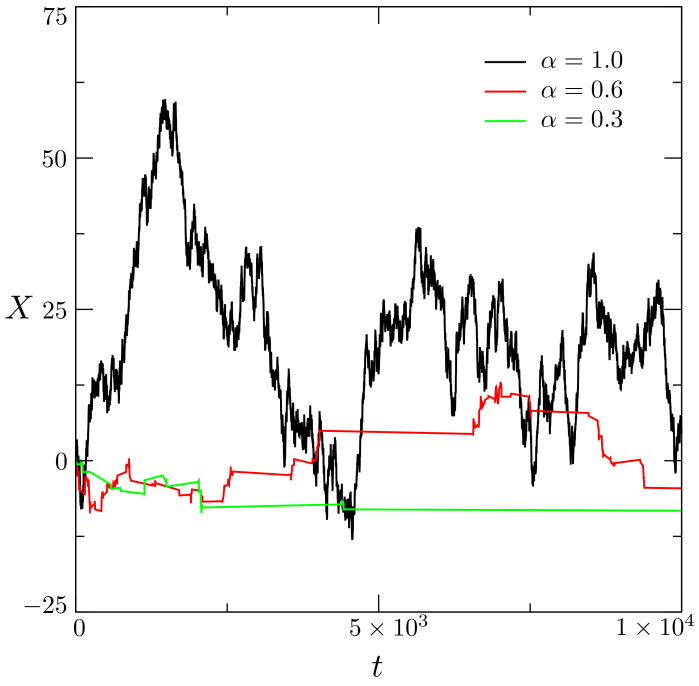

Figure C.1: Examples of trajectories for a RW process ($\alpha = 1$) in black. Also, for two distinct CRTW processes considering a relatively not so long trap-time ($\alpha = 0.6$) in red, and a long trap-time ($\alpha = 0.3$) in green. The time-axis was chosen to be linear to properly show the different trap-times that arrive from the relation (C.5).

From figure C.1 we can appreciate that the diffusive behaviour in CTRW is due the trap-times that the particle goes trough. The case of diffusion in the SM is analogous, a particle tend to follow an unstable manifold, but suddenly it can reach a place that is near the action of an stable manifold. This makes the particle enter the vicinity of a resonance islands and stay trapped there an unpredictable amount of time, due the nature of chaotic dynamics. After some iterations, the particle either escapes from the effect of that resonance island or enters in the effect of another smaller resonance island. This trapping/releasing dynamics of the many manifolds, that are born in the Cantori, makes the particle follow a CTRW-like dynamics.

C.2 Validity of the scaling relation on our mappings

The Shannon entropy is given by:

$$S = -\int_a^b \rho(x,t)\ln(\rho(x,t))\,dx, \tag{C.20}$$

let us consider an scaling relation (C.1) located around the point x_0, i. e.:

$$\rho(x,t) = \frac{1}{t^\delta}F\left(\frac{x-x_0}{t^\delta}\right), \tag{C.21}$$

using this scaling in eq. (C.20) we find:

$$\begin{aligned} S &= -\int_a^b \frac{1}{t^\delta}F\left(\frac{x-x_0}{t^\delta}\right)\ln\left(\frac{1}{t^\delta}F\left(\frac{x-x_0}{t^\delta}\right)\right)dx \\ &= -\int_a^b F\left(\frac{x-x_0}{t^\delta}\right)\ln\left(F\left(\frac{x-x_0}{t^\delta}\right)\right)\frac{dx}{t^\delta} - \int_a^b F\left(\frac{x-x_0}{t^\delta}\right)\ln\left(\frac{1}{t^\delta}\right)\frac{dx}{t^\delta}. \end{aligned}$$

Making the change of variable $u = \frac{x-x_0}{t^\delta}$ we get:

$$S = -\int_{u_a}^{u_b} F(u)\ln(F(u))\,du + \delta\ln(n)\int_{u_a}^{u_b} F(u)\,du,$$

where $u_a = \frac{a-x_0}{t^\delta}$ and $u_b = \frac{b-x_0}{t^\delta}$. Note that $\int_{u_a}^{u_b} F(u)\,du = 1$ since $F(u)$ it is an unknown normalized probability distribution. With this in mind we get the entropy-time relation:

$$S = \delta\ln(t) + A, \tag{C.22}$$

where the second term in the r.h.s. is

$$A = -\int_{u_a}^{u_b} F(u)\ln(F(u))\,du \tag{C.23}$$

whose value in principle has a time dependence trough u_a and u_b. Nevertheless, this time dependence can be dropped out if $a = x_0$ and $b \to \infty$.

We give the following remarks

- Our demonstration of equation (C.22) considers that the diffusion is in one dimension.

- The entropy grows with the logarithm of the time if the diffusion is in the range $[x_0, \infty)$, where x_0 is the location parameter of the scaling (C.21).

Remember the diffusion process for the Simplified Fermi Ulam Model shown in figure C.2.

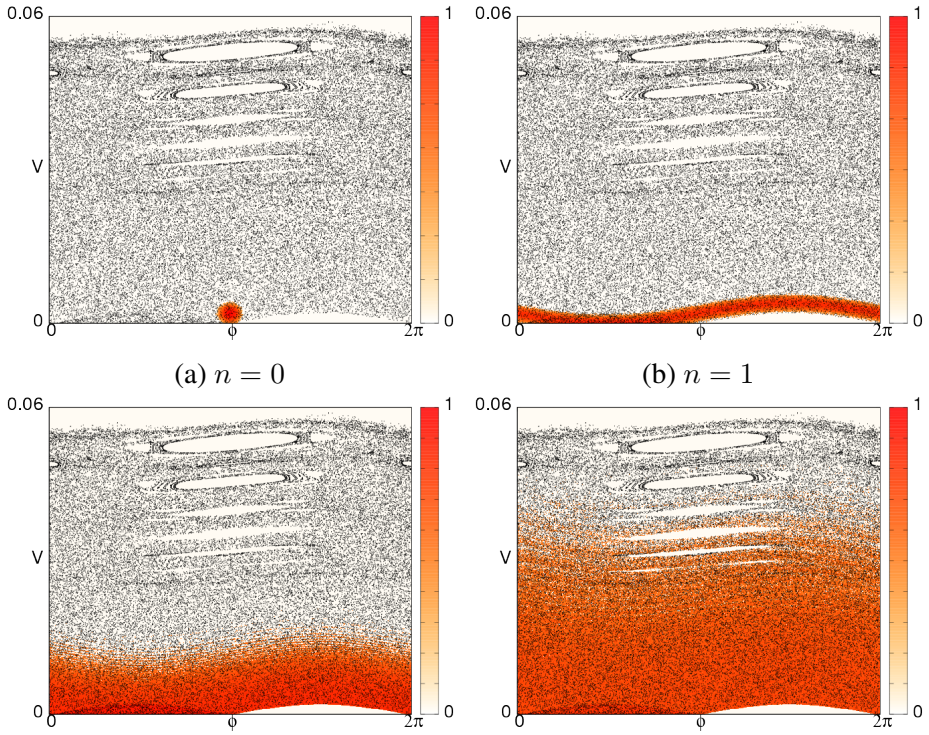

(a) $n = 0$ (b) $n = 1$

(c) $n = 10$ (d) $n = 100$

Figure C.2: Plot of the behaviour of the diffusion process, measured by the probability density, in a chaotic region of phase space for the Simplified Fermi-Ulam Model $\epsilon = 0.001$, for different numbers of iterations n. The orange-white color scale represents the density of points in phase space. The subplots (a) to (d) shows the diffusion process.

We see in figure C.2 that the initial distribution ($n = 0$ in figure C.2a) is centered around a point, and after only one iteration it spreads out totally along the ϕ axis ($n = 1$ in figure C.2b). In the next iterations the points diffuse along the V axis while remaining almost spread along ϕ axis ($n = 10$ and $n = 100$ in figure C.2c and C.2d). We can

notice two things, first the diffusion is effectively one dimensional, specifically in the V variable. Second, for low number of iterations the ensemble is mostly distributed far away from the upper boundary $V_{max} = 2\sqrt{\epsilon}$, even more, by construction the initial ensemble is located in the lower boundary $V_min = 0$. Thus, for low number of iterations we expect that entropy grows with the logarithm of the time, eq. (C.22). This can be appreciated in figure C.3

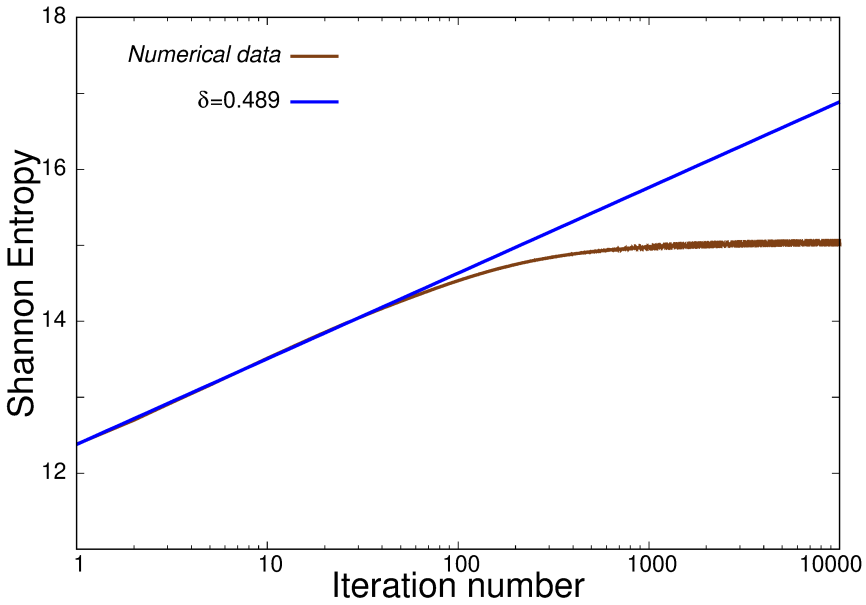

Figure C.3: Plot of the entropy vs. iteration number. For $n < 100$ the numerical data shows a diffusive regime and a plateau for $n > 100$. We also show the value of the diffusion exponent δ after performing a fit with function $S = A + \delta \ln(n)$ in the diffusive regime.

Figure C.3 shows the entropy behaviour from the diffusion process of figure C.2. For $n < 100$ we see a diffusive regime where the entropy grows with the logarithm of the time, then for $n > 100$ the entropy reaches a plateau, this because the ensemble is not longer distributed far away from the upper boundary, this means that the A term of equation (C.22) is not longer a constant.

The diffusion process in the Standard Map is more complicated, see figure C.4

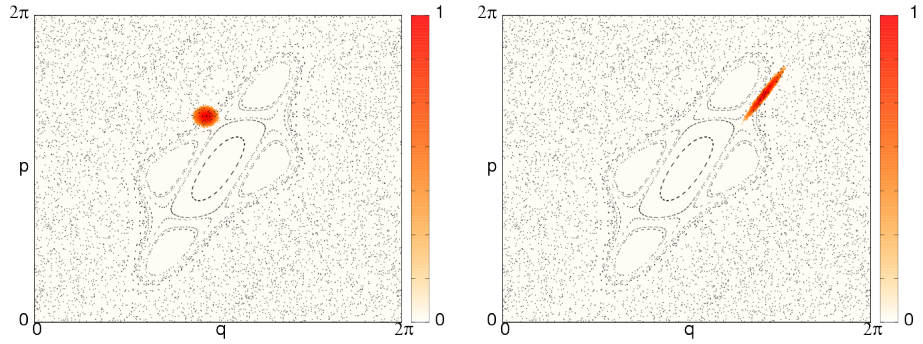

(a) $n = 0$

(b) $n = 1$

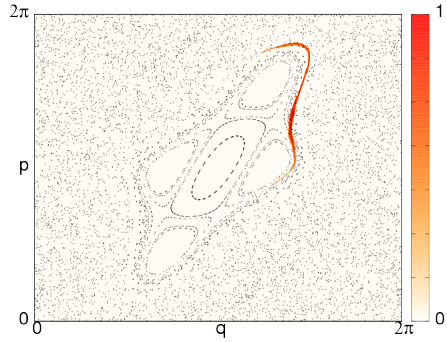

(c) $n = 10$

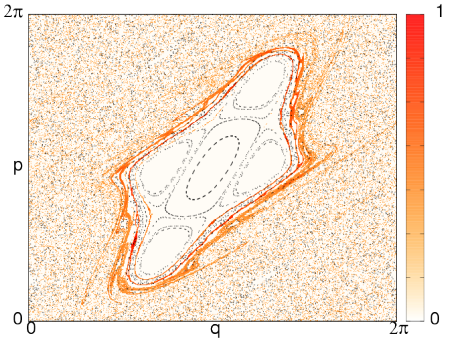

(d) $n = 100$

Figure C.4: Plot of the behaviour of the diffusion process, measured by the probability density, in a chaotic region of phase space for the Standard Map $k = 2.3$, for different numbers of iterations n. The orange-white color scale represents the density of points in phase space. The subplots (a) to (d) shows the diffusion process.

It is possible to see in figure C.4 that the probability distribution first spreads along the shore of the KAM islands and then diffuses outwards. Let us assume that there is a set of canonical variables x, y such that the spreading along the island is roughly described by a diffusion along the variable y, and the diffusion outwards the island is roughly described by a diffusion along the variable x. If there exist such a set of variables, then the entropy growth should allow us to determinate the diffusion exponent if we are studying an *appropriate ensemble*. Note the entropy does not depend on the variables, it can be measured using q and p with out any change, but the entropy growth of equation C.22 depends on the ensemble. Thus, is rather more important to establish the *appropriate ensemble* than the canonical variables.

Inside the island we have the presence of invariant curves, a natural way to choose the canonical variables in this case is to label each invariant curve with an action an-

gle variable x, and every point of the invariant curve corresponds to a different angle variable y, this canonical variables can be extrapolated to outside the island, in [24, 25] show a numerical method to achieve this. Observe that inside the island an ensemble of particles along the same invariant curve will spread in the y variable, while its x coordinate will not change. An ensemble of particles in the shore of the main island will behave in similar way for a small number of iterations. For this reason we choose an ensemble of particles along the shore of the main island. After a small number of iterations they will spread in the whole shore, y coordinate. For the following iterations, our dynamic is reduced effectively to just one dimension, diffusion in the x coordinate. Even more, the initially the ensemble is located in the border of the island, and considering that for small number of iterations does not leaks to much outside the island, we have have established the conditions in which we have the *appropriate ensemble* to use equation (C.22). This description of the dynamics can be seen in figure C.5.

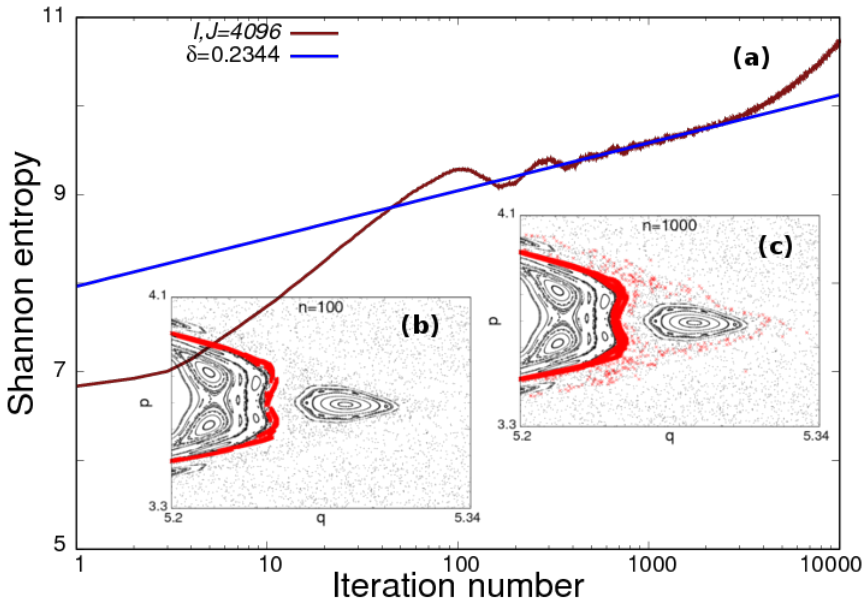

Figure C.5: Plot of the entropy vs. iteration number for $k = 1.31$. The entropy has three growth regimes, i) in the first 100 iterations the distribution spreads along the main island, ii) then for 3000 iterations slowly leaks out through the Cantori, iii) finally more of the distribution is outside the Cantori and rapidly spreads in the chaotic sea.

We show in figure C.5a the entropy behaviour as the time passes. We can recognize three growth regimes: i) First the distribution quickly spreads along the shore of the

main island, y coordinate. This is a fast process equivalent to the spreading in the phase direction in the SFMU, shown in the transition from figure C.2a to figure C.2b. We can appreciate this in the sub-figure 4.4b, that shows how is distributed our ensemble of trajectories after $n = 100$ iterations. ii) The second regime is a slow one, the distribution leaks through the Cantori, x coordinate, see sub-figure C.5c, this is a regime of subdiffusion where we have the conditions to use eq. (C.22). Here we measure the diffusion exponent δ, the numerical fit is shown in a blue line. iii) In the third regime more of the distribution is outside the Cantori and rapidly spreads in the chaotic sea. A fourth regime, not shown in figure C.5, exists, when the ensemble of trajectories is almost uniformly distributed in the chaotic sea, similar to figure C.3, the entropy reaches a plateau.

Appendix D

Entropy and time irreversibility, some comments

D.1 Entropy conservation

Recall Hamilton's equation of motion

$$\begin{aligned} \dot{q} &= \frac{\partial H}{\partial p} , \\ \dot{p} &= -\frac{\partial H}{\partial q} , \end{aligned} \tag{D.1}$$

H is the Hamiltonian, q and p are the canonical conjugate variables. Define V as:

$$V = (\dot{q}, \dot{p}) , \tag{D.2}$$

i. e. the phase space velocity of the representative point[1] $X = (q, p)$. If we have an ensemble of systems, following the same set of equations (D.1), the phase space density ρ of representative points around X behaves like:

$$\frac{\partial \rho}{\partial t} + \nabla \cdot (V\rho) = 0 . \tag{D.3}$$

[1] X represents a system following the dynamics of Hamilton's equations, in our case the trajectory of a particle in phase space.

this is the continuity equation that describe the flow of representative points from one region to another. From equations (D.1) we see that $\nabla \cdot V = 0$, then, the continuity equation (D.3) becomes Liuville's equation [68]:

$$\frac{\partial \rho}{\partial t} + \dot{q}\frac{\partial \rho}{\partial q} + \dot{p}\frac{\partial \rho}{\partial p} = 0 \,. \tag{D.4}$$

The Shannon Entropy is given by:

$$\begin{aligned} S &= -\int dqdp\, \rho \ln(\rho) \\ &= E(-\ln(\rho)) \,, \end{aligned} \tag{D.5}$$

last equation says that S is the expected value of $-\ln(\rho)$. Its time derivative is given by:

$$\begin{aligned} \frac{\partial S}{\partial t} &= E\left(-\frac{\partial \ln(\rho)}{\partial \rho}\frac{\partial \rho}{\partial t}\right) \\ &= E\left(\frac{1}{\rho}\nabla \cdot (V\rho)\right) \\ &= \int dqdp\, \nabla \cdot (V\rho) \\ &= \oint ds \cdot V\rho \\ \frac{\partial S}{\partial t} &= 0 \,, \end{aligned} \tag{D.6}$$

where we used the Divergence Theorem, and the fact that either $\rho \to 0$ when $q, p \to \infty$ or $\oint ds \cdot V\rho = 0$ in periodical boundary conditions. The result of eq. (D.6) says that the Shannon Entropy is a constant in time. So it seems that we can not use the relation $S = A + \delta \ln(t)$ in Hamiltonian Systems. Even more, it seems that the Second Law of Thermodynamics and Hamiltonian systems do not go together.

D.2 Entropy growth

The usual approach to overcome the problem form last section is to study the effects of the coarse grained entropy. Define the function $s(\rho)$ as:

$$s = -\rho \ln(\rho) \ , \tag{D.7}$$

see that $\frac{\partial^2 s}{\partial \rho^2} \leq 0$, then s is a concave function and, by definition of concave functions, the following relation holds:

$$x s(\rho_1) + (1-x)\, s(\rho_2) \ \leq \ s(x\rho_1 + (1-x)\,\rho_2) \ , \tag{D.8}$$

interpreting $0 \leq x \leq 1$ as a weight last equation becomes:

$$\overline{s}(\rho) \leq s(\overline{\rho}) \ , \tag{D.9}$$

which means that the average of s is less or equal than taking s of the averaged ρ. Then, when considering all contributions of s, and averaging at each time step, we have the following equation for the coarse grained entropy $\overline{S}$:

$$\frac{d\overline{S}}{dt} \ \geq \ 0 \, , \tag{D.10}$$

this means that the entropy growth, in Hamiltonian Systems, is due the fact that the probability density is being coarse grained. This averaging is natural to happen in chaotic systems due the stable/unstable manifold's squeezing/expanding action.

D.3 Time reversibility and time irreversibility

Hamiltonian systems at particles level are time reversible, even more, since the equations of motion preserve the phase space area, the entropy of an ensemble of particles, representation points, must be conserved. The averaging process in last section is time irreversibility and this produced an entropy growth. although from a practical point of view this averaging process is paussible, specially due the manifold's dynamics, is still controversial from a physical point of view, since, in principle, we do not know how to

interpret the entropy growth. To understand more this behaviour, we focus in studying the evolution of the probability density rather than representative points.

Without loss of generality let us consider the discrete mapping $x_n = F(x_{n-1})$, then, the evolution of the point x_0 after one iteration can be described in terms of Dirac delta function as:

$$\delta(x - F(x_0)) = \int dx' \, \delta(x - F(x')) \, \delta(x' - x_0) \ , \tag{D.11}$$

since by superposition we have $\rho(x,n) = \int dx_0 \, \delta(x - x_0) \, \rho(x_0, n)$, we obtain terms of Dirac delta function as:

$$\begin{aligned} \rho(x, n+1) &= \int dx' \, \delta(x - F(x')) \, \rho(x', n) \\ &= U\rho(x,n) \ , \end{aligned} \tag{D.12}$$

which defines the operator U, Perron Frobenius operator[2], that evolves densities. If the mapping $x_{n+1} = F(x_n)$ preserves some measure and is time reversible, then U is unitary in Hilbert Space [71], which means that in this space its eigenvalues are of modulus one. In this case the density behaves like:

$$\rho(x,n) = \sum_{k=0}^{\infty} a_k e^{iw_k n} \psi_k(x) \ , \tag{D.13}$$

where e^{iw_k}, $\psi_k(x)$, are the eigenvalues, eigenvectors, of the Perron-Frobenius operator, a_k are constants related to the initial value $\rho(x,0)$. In this solution apparently there is no decay to an equilibrium density, nevertheless, in chaotic systems, we know that densities in the chaotic sea decay to an equilibrium density that fills the whole chaotic sea. For this observation is necessary to use the Resolvent of the Perron Frobenius operator [69, 70], which will bring us to other functional spaces rather than Hilbert Space [71]. For more on the mathematical method and application to hyperbolic maps see refs [71, 73], although for non hyperbolic maps there is no mathematical justification to use the Resolvent, in ref [72] show that finite approximations of the Perron-Frobenius operator give interesting results when studying correlations in chaotic non hyperbolic

[2]This is the analogous of Liuville's operator for general systems

maps.

We highlight some physical relevant results of the bibliography:

1. The functional spaces of U appropriate for forward time evolution and backward time evolution, are different, meaning that there is an asymmetry in the time evolution [71, 73].

2. For some systems, trajectories are not possible to recover from the spectral decomposition of U, this because trajectories correspond to non-differentiable point densities. Thus, by considering a representation of the system were we care about densities rather than trajectories, the dynamical laws include time irreversibility, which do not contradict the time reversibility at trajectory level. Then, since the representation that breaks time symmetry is in accordance with or experience of nature it might be that trajectories must be seen as *stochastic realizations* of the more fundamental probability densities, [71].

Since entropy is related to probability densities and not trajectories, it is expected that it grows in a time irreversible dynamic.

Bibliography

[1] I. Newton, *Philosophiae Natvralis Principia Mathematica*. London, 1687.

[2] H. Poincaré. *Les méthodes nouvelles de la mécanique céleste*. Gauthier-Villars it fils, 1892-1899.

[3] K. F. Sundman, "Mémoire sur le problème des trois corps". Acta Mathematica, vol. 36, pp. 105, 1913.

[4] W. Qiu-Dong, "The global soltion of the n-body problem". Celestial Mechanics and Dynamical Astronomy, vol. 50, pp. 73, 1990.

[5] F. Dicau, "The solution of the n-body problem". The Mathematical Intelligencer, vol. 18, pp. 66, 1996.

[6] E. N. Lorenz "Deterministic nonperiodic flow". Journal of the atmospheric sciences, vol.20, pp. 130, 1963.

[7] M. J. Feigenbaum "The universal metric properties of nonlinear transformations". Journal of Statistical Physics, vol. 21, pp. 669, 1979.

[8] S. H. Strogatz, *Nonlinear dynamics and chaos: with applications to physics, biology, chemistry and engineering*. Westviez press, 2014.

[9] G. M. Zaslavsky, *Physics of Chaos in Hamiltonian Systens*, Imperial College Press, New York, 2007.

[10] M. F. Shlesinger, G. M. Zaslavsky and J. Klafter, "Strange Kinetics". Nature, vol. 363, pp. 31, 1993.

[11] C. P. Dettmann, “Diffusion in the Lorentz gas”. Commun. in Theoretical Physics vol. 62, No. 4, pp. 521, 2014.

[12] E. Fermi, “On the Origin of the Cosmic Radiation”. Phys. Rev., vol. 75, No. 8, pp. 1169, 1949.

[13] A. J. Litchenberg, M. A. Lieberman and R. H. Cohen, “Fermi acceleration revisted”. Physica D, vol. 1, pp. 291, 1980.

[14] S. O. Kamphorst, E. D. Leonel and J.K.L. Da Silva, “The presence and lack of Fermi acceleration in nointegrable billiards”. Journal of Physics A, vol 40, p. F887, 2007.

[15] R. S. MacKay, J. D. Meiss, I. C. Percival, “Transport in Hamiltonian systems”. Physica D, vol. 13, pp. 55, 1984.

[16] N. B. de Faria, D. S. Tavares, W. C. de Paula, E. D. Leonel and D. G. Ladeira, “Transport of chaotic trajectories from regions distant from or near to structures of regular motion of the Fermi-Ulam model”. Physical Review E, vol. 94, pp. 042208, 2016.

[17] M. Roberto, E. C. Silva, I. L. Caldas and R. L. Viana, “Magnetic trapping caused by resonant perturbations in tokamaks with reversed magnetic shear”, Phys. Plasmas vol. 11, pp. 214, 2004.

[18] C. G. L Martins, M. Roberto and I. L. Caldas, “Magnetic field line stickiness in tokamaks”, IEEE TRANSACTIONS ON PLASMA SCIENCE, vol. 42, pp. 2764, 2014.

[19] D. F. Oliveira, M. R. Silva and E. D. Leonel, “A symmetry break in energy distribution and a biased random walk behavior causing unlimited diffusion in a two dimensional mapping”. Physica A, vol. 436, pp. 909, 2015.

[20] A. L. P. Livorati, T. Kroetz, C. P. Dettmann, I. L. Caldas e E. D. Leonel, “Stickiness in a Bouncer model: a slowing mechanism for Fermi acceleration”, Phys. Rev. E, vol. 86, pp. 036204, 2012.

[21] G. M. Zaslavsky, “Chaos, fractional kinetics, and anomalous transport”. Phys Rep., vol. 371, pp. 461, 2002.

[22] E. D. Leonel, J. A. De Oliveira and F. Saif, “Critical exponents for a transition from integrability to non-integrability via localization of invariant tori in the Hamiltonian system”. Journal of Physics A, vol. 44, pp. 302001, 2011.

[23] M. S. Palmero, G. I. Díaz, P. V. McClintock and E. D. Leonel, “Diffusion Phenomena in a Mixed Phase Space”. 2019.

[24] A. Bäcker, R. Ketzmerick and S. Löck, “Direct regular-to-chaotic tunneling rates using the fictitious-integrable-system approach”. Physical Review E, vol. 82, pp. 05608, 2010.

[25] C. Löbner, S. Löck, A. Bäcker and R. Ketzmerick “Integrable approximation of regular islands: The iterative canonical transformation method”. Physicial Review E, vol. 88, pp. 062901, 2013.

[26] A. N. Kolmogorov “On the Conservation of Conditionally Periodic Motions under Small Perturbation of the Hamiltonian”. Dokl. Akad. Nauk. SSR., vol. 98, pp 2, 1954.

[27] J. Moser, “On invariant curves of area-preserving mappings of an annulus”. Nachr. Akad. Wiss. II, pp. 1, 1962.

[28] V. I. Arnold, “Proof of a theorem of A. N. Kolmogorov on the preservation of conditionally periodic motions under a small perturbation of the Hamiltonian”. Uspekhi Mat. Nauk, vol. 18, 1963 (English transl. ¿ Russ. Math. Surv, vol. 18).

[29] I. C. Percival, “A variational principle for invariant tori of fixed frequency”. Journal of Physics A: Mathematical and General, vol. 12, 1979.

[30] N. Scafetta and P. Grigolini, “Scaling detection in time series: diffusion entropy analysis”. Physical Review E, vol. 66, pp. 036130, 2002.

[31] C. E. Shannon, “A mathematical theory of communication”. Bell System technical Journal, vol. 27, pp. 379, 1948.

[32] A.Lesne, “Shannon entropy: A rigorous notion at the crossroads between probability, information theory, dynamical systems and statistical physics”. Mathematical Structures in Computer Science, vol. 24, 2014.

[33] B. V. Chirikov, “Research concerning the theory of nonlinear resonance and stochasticity”. Preprint N 267, Institute of Nuclear Physics, Novosibirsk, 1969, (Engl. Trans., CERN Trans. 71-40 1971).

[34] B. V. Chirikov, “A universal instability of many-dimensional oscillator systems”. Phys. Rep. vol. 52, pp. 263, 1979.

[35] M. V. Berry, “Regularity and chaos in classical mechanics, illustrated by three deformations of a circular billiard”. Eur. J. Phys. vol. 2, pp. 91-102, 1981.

[36] R. C. Hilborn, *Chaos and Nonlinear Dynamics: An Introduction for Scientists and Engineers*. Oxford University Press, New York, 1994.

[37] A. J. Lichtenberg, M.A. Lieberman, *Regular and Chaotic Dynamics*. Appl. Math. Sci. 38, Springer Verlag, New York, 1992.

[38] G. M. Zaslavsky, *Hamiltonian Chaos and Fractional Dynamics*, Oxford University Press, New York, 2008.

[39] D. Ciro, I. L. Caldas, R. L. Viana and T. E. Evans, “Efficient manifold tracing for planar maps” Chaos: An Interdisciplinary Journal of Nonlinear Science vol. 28, pp. 093106, 2018.

[40] L. A. Bunimovich, “On Ergodic Properties of Certain Billiards”. Funct. Anal. Appl., vol. 8, pp. 254, 1974.

[41] N. Chernov and R. Markarian, *Chaotic Billiards*. American Mathematical Society, Vol. 127, 2006.

[42] C. P. Dettmann, “Recent advances in open billiards with some open problems”. Frontiers in the study of chaotic dynamical systems with open problems, pp. 195, 2011.

[43] G. D. Birkhoff, “On the periodic motions of dynamical systems”, Acta Mathematica, vol. 50, pp. 359, 1927.

[44] Y. G. Sinai,“Dynamical systems with elastic reflections”. Russ. Math. Surveys., vol. 25, pp. 137, 1970.

[45] N. Krylov, *Works on the Foundations of Statistical Physics* Princeton Univ. Press, Princeton, NJ, 1979.

[46] J. Skowron, A. Gould, “General complex polynomial root solver and its futher optimizarion for binary microlenses”. arXiv preprint arXiv:1203.1034, 2012

[47] J. L. Lagrange, “Réflexions sur la résolution algébrique des équations”. CEuvres de Lagrange, III, Gauthier-Villars, pp. 205, 1869.

[48] F. W. J. Olver, A. B. Olde Daalhuis, D. W. Lozier, B. I. Schneider, R. F. Boisvert, C. W. Clark, B. R. Miller, and B. V. Saunders, eds., “Digital Library of Mathematical Functions”. http://dlmf.nist.gov/, Realese 1.0.22 of 2019-03-15.

[49] F. T. Krogh, C. L. Lawson, and W. Van Snyder, eds., “MATH77 and mathc90, Realese 6.0. Libraries of Mathematical Subprograms in Fortran 77 and C”. California Institute of Technology, 1998.

[50] E. D. Leonel, P. V. McClintock and J. K. L. da Silva, “Fermi-Ulam accelerator undes scaling analysis”. Physical Review Letters, vol. 93, pp. 014101, 2004.

[51] P. Dierckx, “Curve and surface fitting with splines”. Oxford University Press, 1995.

[52] S. Lange, M. Richter, F. Onken, A. Bäcker, R. Ketzmerick, “Global structure of regular tori in a generic 4D sympletic map”. Chaos: An Interdisciplinary Journal of Nonlinear Science, vol. 24, pp. 024409, 2014.

[53] G. D. Birkhoff, “An extension of Poincaré’s last geometric theorem”. Acta. Math., vol. 47, pp. 297, 1925.

[54] Y. S. Sun, L. Zhou and J. L. Zhou, “The role of hyperbolic invariant sets in stickiness effects”, in *A Comparison of the Dynamical Evolution of Planetary Systems*, Springer, Dordrecht, 2005.

[55] T. S. Kruger, P. P. Galuzio, T. D. L. Prado, R. L. Viana, J. D. Jr. Szezech and S. R. Lopes, “Mechanism for stickiness suppression during extreme events in Hamiltonian systems”. Physical Review E, vol.91, pp. 062903, 2015.

[56] G. Contopoulos and M. Harsoula, “Stickiness effects in chaos”. Celestial Mechanics and Dynamical Astronomy, vol. 107, pp. 77, 2010.

[57] S. Tomsovic, “Tunneling and Chaos”. Physica Scripta, no. T90 pp. 162, 2001.

[58] M. J. Davis and E. J. Heller, “Quantum dynamical tunneling in bound states”. The Journal of Chemical Physics, no. 1, pp. 246, 1981.

[59] Y. Meroz, and I. Sokolov, “A toolbox for determining subdiffusive mechanisms”. Physics Reports, vol. 573, pp. 1, 2015.

[60] B. B. Mandelbrot, and J. W. Van Ness, “Fractional Brownian motions, fractional noises and applications”. SIAM review, vol. 10, no. 4, pp. 422, 1968.

[61] H. Scher, and E. W. Montroll, “Anomalous transit-time dispersion in amorphous solids”. Physical Review B, vol. 12, no. 6, pp. 2455, 1975.

[62] G. M. Zaslavsky, M. Edelman, and B. A. Niyazov, “Self-similarity, renormalization, and phase space nonuniformity of Hamiltonian chaotic dynamics”. Chaos: An Interdisciplinary Journal of Nonlinear Science, vol. 7, no. 1, pp. 159, 1997.

[63] I. M. Sokolov, and J. Klafter, “From diffusion to anomalous diffusion: a century after Einstein’s Brownian motion”. Chaos: An Interdisciplinary Journal of Nonlinear Science vol. 15, pp. 026103, 2005.

[64] R. Balescu, *Statistical Dynamics: Matter Out of Equilibrium*, Imperial College Press, 1997.

[65] M. Magdziarz, A. Weron, and K. Weron,“Fractional Fokker-Planck dynamics: Stochastic representation and computer simulation”. Physical Review E, vol. 75, pp. 016708, 2007.

[66] A. Janicki, A. Weron, *Simulation and chaotic behaviour of α-stable stochastic processes*, CRCPress, 1993.

[67] H. J. Haubol, A. M. Mathai, and R. K. Saxena, “Mittag-Leffler functions and their applications”. Journal of Applied Mathematics, vol. 2011, pp. 298628, 2011.

[68] H. Goldstein, C. Poole, and J. Safko, *Classical mechanics*, 2002.

[69] M. Pollicott, “On the rate of mixing of Axiom A flows”. Inventiones mathematicae, vol. 81, no. 3, pp. 413, 1985.

[70] D. Ruelle, “Resonances of chaotic dynamical systems”. Physical review letters, vol. 56, no. 5, pp. 405, 1986.

[71] D. J. Driebe, *Fully chaotic maps and broken time symmetry*. Springer Science and Business Media, 1999.

[72] S. Fishman, and S. Rahav, “Relaxation and noise in chaotic systems”. In *Dynamics of Dissipation*, Springer, Berlin, Heidelberg, pp. 165, 2002.

[73] S. Tasaki, “Irreversibility in reversible multibaker maps-Transport and fractal distributions”. Advances in Chemical Physics, vol. 122, pp. 77, 2002.